REPORT DOCUMENTATION PAGE

Public reporting burden for this collection of information is estimated to average 1 hour per response, including the time for reviewing instructions, searching existing data sources, gathering and maintaining the data needed, and completing and reviewing the collection of information. Send comments regarding this burden estimate or any other aspect of this collection of information, including suggestions for reducing this burden, to Washington Headquarters Services, Directorate for Information Operations and Reports, 1215 Jefferson Davis Highway, Suite 1204, Arlington, VA 22202-4302, and to the Office of Management and Budget, Paperwork Reduction Project (0704-0188), Washington, DC 20503.

1. AGENCY USE ONLY (Leave blank)	2. REPORT DATE July 96	3. REPORT TYPE AND DATES COVERED

4. TITLE AND SUBTITLE
Silicon Nitride Joining Using a Sr-Celsian-Based Glass Interlayer

5. FUNDING NUMBERS

6. AUTHOR(S)

Brian Grant Quillen

7. PERFORMING ORGANIZATION NAME(S) AND ADDRESS(ES)

AFIT Student Attending:

University of New Mexico

8. PERFORMING ORGANIZATION REPORT NUMBER

96-042

9. SPONSORING/MONITORING AGENCY NAME(S) AND ADDRESS(ES)
DEPARTMENT OF THE AIR FORCE
AFIT/CI
2950 P STEET, BLDG 125
WRIGHT-PATTERSON AFB OH 45433-7765

10. SPONSORING/MONITORING AGENCY REPORT NUMBER

11. SUPPLEMENTARY NOTES

12a. DISTRIBUTION/AVAILABILITY STATEMENT
Approved for Public Release IAW 190-1
Distribution Unlimited
BRIAN D. GAUTHIER, MSgt, USAF
Chief Administration

12b. DISTRIBUTION CODE

13. ABSTRACT (Maximum 200 words)

19960809 072

14. SUBJECT TERMS	15. NUMBER OF PAGES 73
	16. PRICE CODE

17. SECURITY CLASSIFICATION OF REPORT	18. SECURITY CLASSIFICATION OF THIS PAGE	19. SECURITY CLASSIFICATION OF ABSTRACT	20. LIMITATION OF ABSTRACT

GENERAL INSTRUCTIONS FOR COMPLETING SF 298

The Report Documentation Page (RDP) is used in announcing and cataloging reports. It is important that this information be consistent with the rest of the report, particularly the cover and title page. Instructions for filling in each block of the form follow. It is important to *stay within the lines* to meet *optical scanning requirements*.

Block 1. Agency Use Only *(Leave blank)*.

Block 2. Report Date. Full publication date including day, month, and year, if available (e.g. 1 Jan 88). Must cite at least the year.

Block 3. Type of Report and Dates Covered. State whether report is interim, final, etc. If applicable, enter inclusive report dates (e.g. 10 Jun 87 - 30 Jun 88).

Block 4. Title and Subtitle. A title is taken from the part of the report that provides the most meaningful and complete information. When a report is prepared in more than one volume, repeat the primary title, add volume number, and include subtitle for the specific volume. On classified documents enter the title classification in parentheses.

Block 5. Funding Numbers. To include contract and grant numbers; may include program element number(s), project number(s), task number(s), and work unit number(s). Use the following labels:

C	-	Contract	PR	-	Project
G	-	Grant	TA	-	Task
PE	-	Program Element	WU	-	Work Unit Accession No.

Block 6. Author(s). Name(s) of person(s) responsible for writing the report, performing the research, or credited with the content of the report. If editor or compiler, this should follow the name(s).

Block 7. Performing Organization Name(s) and Address(es). Self-explanatory.

Block 8. Performing Organization Report Number. Enter the unique alphanumeric report number(s) assigned by the organization performing the report.

Block 9. Sponsoring/Monitoring Agency Name(s) and Address(es). Self-explanatory.

Block 10. Sponsoring/Monitoring Agency Report Number. *(If known)*

Block 11. Supplementary Notes. Enter information not included elsewhere such as: Prepared in cooperation with...; Trans. of...; To be published in.... When a report is revised, include a statement whether the new report supersedes or supplements the older report.

Block 12a. Distribution/Availability Statement. Denotes public availability or limitations. Cite any availability to the public. Enter additional limitations or special markings in all capitals (e.g. NOFORN, REL, ITAR).

DOD	- See DoDD 5230.24, "Distribution Statements on Technical Documents."
DOE	- See authorities.
NASA	- See Handbook NHB 2200.2.
NTIS	- Leave blank.

Block 12b. Distribution Code.

DOD	- Leave blank.
DOE	- Enter DOE distribution categories from the Standard Distribution for Unclassified Scientific and Technical Reports.
NASA	- Leave blank.
NTIS	- Leave blank.

Block 13. Abstract. Include a brief *(Maximum 200 words)* factual summary of the most significant information contained in the report.

Block 14. Subject Terms. Keywords or phrases identifying major subjects in the report.

Block 15. Number of Pages. Enter the total number of pages.

Block 16. Price Code. Enter appropriate price code *(NTIS only)*.

Blocks 17. - 19. Security Classifications. Self-explanatory. Enter U.S. Security Classification in accordance with U.S. Security Regulations (i.e., UNCLASSIFIED). If form contains classified information, stamp classification on the top and bottom of the page.

Block 20. Limitation of Abstract. This block must be completed to assign a limitation to the abstract. Enter either UL (unlimited) or SAR (same as report). An entry in this block is necessary if the abstract is to be limited. If blank, the abstract is assumed to be unlimited.

Brian Grant Quillen

Candidate

Chemical and Nuclear Engineering Department

Department

This thesis is approved, and it is acceptable in quality
and form for publication on microfilm:

Approved by the Thesis Committee:

_Ronald Loehman_____ , Chairperson

_Werner Lutze_____

_William Falnoff_____

_____

_____

_____

_____

_____

Accepted:

_____
Dean, Graduate School

_____
Date

Silicon Nitride Joining Using a

Sr-Celsian-Based Glass Interlayer

by

Brian Grant Quillen

B.S. Chemical Engineering, University of Arkansas, 1990

M.S. Chemical Engineering, University of New Mexico, 1996

THESIS

Submitted in Partial Fulfillment of the
Requirements for the Degree of

The University of New Mexico
Albuquerque, New Mexico

July, 1996

DEDICATION

This research thesis is dedicated to my beautiful and loving wife Maria Ana and to our newborn son, Blake William, who was born during my graduate study.

ACKNOWLEDGMENTS

Silicon Nitride Joining Using a

Sr-Celsian-Based Glass Interlayer

by

Brian Grant Quillen

B.S. Chemical Engineering, University of Arkansas, 1990

M.S. Chemical Engineering, University of New Mexico, 1996

ABSTRACT OF THESIS

Submitted in Partial Fulfillment of the
Requirements for the Degree of

The University of New Mexico
Albuquerque, New Mexico

July, 1996

Silicon Nitride Joining Using a
Sr-Celsian-Based Glass Interlayer

by

Brian Grant Quillen

B.S. Chemical Engineering, University of Arkansas, 1990.

M.S. Chemical Engineering, University of New Mexico, 1996.

ABSTRACT

Si_3N_4 was successfully joined to itself using a SiO_2-SrO-Al_2O_3 glass composition. Two compositions were evaluated as joining agents, designated SAS-5 and SAS-10 with compositions of 51:44:5 and 49:41:10 weight % SiO_2:SrO:Al_2O_3, respectively. Microstructure of the joint region was examined by electron microprobe and X-ray diffraction. Contact angle measurements and glass characterization, including differential thermal analysis (DTA), dilatometer thermal expansion measurements and crystallization experiments, were used to evaluate each glass composition. Si_3N_4 plates were joined using interlayers of SAS-5 and SAS-10 glass powder ground to 75 μm particle size. Joining was carried out at 1450 °C in a flowing N_2 atmosphere with an applied load of only 0.01 MPa for each glass. Maximum room temperature strengths of 470 and 378 MPa were achieved in four-point bending tests for the SAS-5 and SAS-10 bonded joints, respectively.

TABLE OF CONTENTS

LIST OF FIGURES

LIST OF TABLES

1 INTRODUCTION

1.1 Industrial Applications of Si_3N_4

Si_3N_4 is an attractive material for structural and advanced turbomachinery applications because of its high temperature strength (above 689 MPa in bending up to 1,000 °C), excellent resistance to thermal shock, low thermal expansion, low thermal conductivity, high hardness, and corrosion resistance (*1*). In gas turbine engine applications, Si_3N_4 offers the advantage of increased turbine inlet temperature and greater range/payload. In addition, it can increase reliability and decrease maintenance through enhanced corrosion resistance and overtemperature capability. A comparison of Si_3N_4 properties to those of metals commonly used for pistons and other engine components is shown in Table 1.

TABLE 1

Comparison of Si_3N_4 and Metal Component Properties (*2*)

	Al alloys[*]	Grey Cast Iron (BS 1452)	Inconel 718[#]	Si_3N_4[+]
Melting point °C	560	930-1230	1400	1750-1900
Strength MPa	190-280	200-300	758[++]	800[**]

* Based on Al alloys LM13 and LM26 as described in (*2*)

Nickel-based superalloy (*3*)

+ Hot pressed Si_3N_4 (fully dense)

++ Tensile Strength

** 3-point bend strength at room temperature

1.2 Defense Department Interest

US Department of Defense (DOD) interest in the area of gas turbine ceramics, and Si_3N_4 in particular, dates back to 1971, when the Advanced Research Projects Agency initiated a program to accelerate ongoing work in that area. A contract was awarded to Ford Motor Company, with Westinghouse Electric Company as a subcontractor, to develop a design capability with brittle materials (i.e. ceramics). Since then, Si_3N_4 components have been demonstrated in applications such as turbocharger rotors, pistons, cylinder liners, combustors, stators, inlet nose cones, and ball bearings (used in the space shuttle main engine high pressure oxidizer turbopump) (*4-6*).

1.3 Si_3N_4 Processing

In spite of its great potential for high temperature applications, Si_3N_4 is limited in terms of the shapes that can be produced without extensive and costly grinding. Hot-pressed Si_3N_4, the strongest type of Si_3N_4, is produced by the application of both heat and uni-axial pressure in graphite dies heated to temperatures in the range of 1650 to 1850 °C for one to four hours. An applied stress of 15 to 30 MPa is typically employed. Boron nitride is applied as a coating to prevent reactions between the graphite die and plungers with the Si_3N_4. Since surface contamination is usually a problem, its likelihood is minimized by pre-pressing the powder mix in a metal die to form a compact prior to introduction into the graphite die. However, the resulting hot-pressed Si_3N_4 is limited to simple-shaped billets and components must be machined from these billets via grinding (a more thorough discussion of Si_3N_4 processing problems is presented by Gugel (*7*)). Because of these limitations on hot-pressed shapes, many applications of hot-pressed Si_3N_4 require it to be joined to itself or to other materials such as metals.

1.4 Si$_3$N$_4$ Joining Methods

There are three general classes of techniques for joining two Si$_3$N$_4$ components. One method uses different reactive braze filler metals, such as Al or Ti-containing alloys. The Si$_3$N$_4$ components are joined using metals and alloys that melt, wet, and react with the ceramic at the interface.

Another technique uses glass or ceramic joining compositions that are chemically compatible with the intergranular phase of the Si$_3$N$_4$. The intergranular phases are formed from the small amounts of MgO, Y$_2$O$_3$, or Al$_2$O$_3$ that are commonly added to densify Si$_3$N$_4$ powders. These additives speed up the necessary chemical reactions at high sintering temperatures by forming refractory glasses that bind the structure. Their presence is significant in the composition of the intergranular phase. The joining glass/ceramic composition is chosen so that it forms a liquid below the decomposition temperature of Si$_3$N$_4$ and wets the surface. With additional time at temperature (typically between 1200 °C and 1600 °C), the Si$_3$N$_4$ grains dissolve in the liquid and counter-diffusion of cations between the glass/ceramic composition and the Si$_3$N$_4$ occurs, resulting in the creation of a joint region that is similar in composition to the original Si$_3$N$_4$ grain boundary phase.

The third method involves diffusion reaction bonding of sintered Si$_3$N$_4$ components (with or without additives) under high pressure and temperature. The joint formed via this technique is very similar in composition to the parent Si$_3$N$_4$ materials.

1.5 Joining Applications and Results

Si$_3$N$_4$ has been successfully joined using each of the techniques described above attaining room temperature strengths above 500 MPa (*8-22*). Iwamoto *et al.* (*18*) demonstrated the use of these Si$_3$N$_4$ joints in structural applications such as curtains for

the hot blast stove used in steel making. McLean and Baker (*23*) presented another example of applied Si_3N_4 joints in the duo-density Si_3N_4 gas turbine rotor. In this case, a reaction bonded Si_3N_4 blade ring is joined to a hot-pressed Si_3N_4 hub.

1.6 Thesis Purpose and Scope

In this research, a SiO_2-SrO-Al_2O_3 glass system was investigated as an agent for joining Si_3N_4 to itself. The primary focus of this research is to identify the joining mechanisms involved in using this glass system. Furthermore, this research was designed to evaluate the thermal stability of the glass with respect to attaining high temperature joint strengths. The advantage of using a SiO_2-SrO-Al_2O_3 glass lies in its potential for crystallizing into monoclinic celsian, with the stoichiometric composition SrO-Al_2O_3-$2SiO_2$, at temperatures above 1,000 °C (*24*). Celsian is thermally stable and possesses a high melting point and low coefficient of thermal expansion (CTE), 2.29×10^{-6}/ °C from 20 °C to 1,000 °C . Room temperature joint strengths demonstrate the compatibility between the glass compositions and the Si_3N_4.

2 LITERATURE REVIEW

2.0 General

The literature review for this research focused on two main areas. The first area involves research on methods for joining Si_3N_4 ceramics, as well as any applications of Si_3N_4 joints. The second area encompasses celsian glass research.

2.1 Types and Systems for Joining Ceramics

The three primary means of joining Si_3N_4 ceramics, as previously mentioned, vary according to the type of joint interlayer employed. Literature review of these joining methods is partitioned according to the joint interlayer employed: braze metal, solid state diffusion bonding without an interlayer, and oxide glass.

2.1.1 Braze Metal Joining Systems

The method of using reactive braze filler metals to join Si_3N_4 components utilizes an oxidation-reduction mechanism. Si_3N_4 pieces are joined using metals and alloys that are thermodynamically reactive with the ceramic components. The metals that react can be predicted using Gibbs energy calculations (a negative Gibbs energy calculation correlates to a feasible reaction).

Suganuma *et al.*(*8*) joined pressureless-sintered Si_3N_4 in Ar using an Al interlayer at temperatures above the melting point of Al and at pressures of 0 to 0.15 MPa. No reaction was observed between the Al and the Si_3N_4 up to 1223 K, although the formation of aluminum nitride or aluminum oxide is possible in this temperature range. Relatively high room temperature bending strengths of 400 to 500 MPa were reported. Al was selected as a bonding agent in an attempt to reduce the necessary bonding temperature, bonding pressure, bonding time, and the cost of the bonding process.

Milberg *et al.* (*9*) joined hot pressed Si_3N_4 and reaction-bonded Si_3N_4 by heating an interlayer of metallic Al and SiO_2 in a nitriding atmosphere. XRD analysis indicated the presence of SiAlON phases in the joints. The bonding reaction involved the reduction of Si_3N_4 by Al and the subsequent renitriding of the resultant Si, as well as the simultaneous nitriding of a portion of the Al. The joints were found to be resistant to thermal shock and maintain their room temperature strength up to 1200 °C.

Although Si_3N_4 joining using a metal-based interlayer is suitable for low temperature, low stress joints, lack of high temperature strength is a major deficiency for this method. There are two primary reasons for the poor high temperature strength of Si_3N_4 joints attained with metal interlayers. One is the mismatch in the CTE between the ceramic and stiff metals. The mean CTE of Si_3N_4 from room temperature to 1000 °C is 3.0×10^{-6}/°C; the mean CTE of tungsten, which has the smallest CTE of all pure metals, is about 4.5×10^{-6}/°C. The second reason involves melting of the alloy at elevated operating temperatures. The low melting points of these metal alloys detracts from their use at high temperatures. These factors cause failures of a joint when they are bonded directly at elevated temperature.

2.1.2 Diffusion Bonding Systems (no metal or glass interlayer)

One means of attaining a match in CTE at the interface of a ceramic-ceramic joint is to bond the pieces at high pressure and at high temperature without using an interlayer. In this method, strong bonds are achieved through solid state diffusion without melting the base materials. Solid state diffusion bonding of Si_3N_4 has been employed to attain relatively high strengths.

Kaba, Shimada, and Koizumi (*10*) successfully joined hot pressed Si_3N_4 by diffusional reaction bonding by maintaining samples at 3.0 GPa and 1800 °C for 1 hour. SEM

examination of the interfaces of the bonded samples reveal an identical microstructure across the parent bodies and the interface. Electron microprobe analysis of the joint region revealed diffusion of Y (from the Y_2O_3 additive in the Si_3N_4) and Si into the interfacial region. Vickers microhardness values of 21.6 GN/m^2 (room temperature) and 12.7 GN/m^2 (1200 °C) were reported for both the parent body and the joint region.

Nakamura *et al.* (*11*) joined hot-pressed Si_3N_4 using polyethylene as a joining agent and applying uni-axial pressure at high temperature. Use of polyethylene in a heated nitrogen atmosphere was intended to leave a certain amount of carbon, which would react with the Si_3N_4 to form a SiC layer between the joined specimens. The effects of joining conditions such as temperature (from 1400 to 1600 °C), joining pressure (0.1 to 40 MPa), holding time (30 min to 8 hours), and surface roughness of the joining couple (about 0.12, 0.22, and 1.2 µm) on the joining strength were studied. Joining strength increased with increases in joining temperature, joining pressure, and holding time. Larger surface roughness caused lower joining strength. The highest joining strength attained was 567 MPa at room-temperature. High temperature strength did not differ much from the strength at room-temperature. In a follow up study, Nakumra and Peteves (*12*) joined hot-pressed Si_3N_4 using this polyethylene joining agent by applying a higher uni-axial pressure at high temperature (10 atm N_2 as opposed to 1 atm N_2). Higher pressure was applied to suppress the decomposition of Si_3N_4 at the imposed high joining temperatures. The maximum joint strength achieved was 666 MPa, considerably higher than the 567 MPa achieved with lower applied pressure.

Sundberg and Ferber (*13*) co-densified joined 4 wt% Y_2O_3-Si_3N_4 bodies via glass encapsulated hot isostatic pressing with self-bonded and slip join interlayers. The slip join interlayer consisted of a composition of the parent 4 wt% Y_2O_3-Si_3N_4 material as a powder suspended in a liquid medium. The self-bonded interlayer was formed by placing

the flat surfaces of the two materials into contact and heating. The joined materials survived 200 hours at 1370 °C under a constant flexural stress of 250 MPa, with a maximum strain of 0.006. Mean room temperature flexure strengths of 881 MPa were reported, compared to an unjoined room temperature flexure strength of 1030 MPa for the parent material.

Although diffusion bonding of Si_3N_4 components achieves a CTE match across the joint interface, and thereby helps produce better high temperature strengths, the process is limiting in terms of forming complex shapes. The shapes formed using this method are limited because of the need to apply high uni-axial pressure at high temperature in a hot isostatic press. Additionally, diffusion bonding requires a longer joining time than other techniques and equipment costs are high due this combination of high temperature and pressure in vacuum environments, as discussed in the review of diffusion bonding by Akselsen (14).

2.1.3 Oxide Glass Joining Systems

A third approach to attaining high strength Si_3N_4 joints at elevated temperatures involves the use of an oxynitride glass interlayer. This approach offers a closer CTE match than metal interlayers and also holds more promising prospects for forming complex shapes.

Becher and Halen (15) joined hot-pressed Si_3N_4 using ZrO_2 and $ZrSiO_4$ powder to form the bonding layer. Bonding was accomplished by heating the sample to temperatures in the range 1400-1550 °C at about 20 °C /min while applying a pressure of ≤ 1.5 MN/m^2. Materials applied to form the bonding layer were selected based on analysis of thermal expansion coefficients. Moderate strength, high-fracture-toughness joints were obtained using a ZrO_2 bond layer and high purity hot-pressed Si_3N_4. Use of a $ZrSiO_4$ bond layer

was not successful in producing a Si_3N_4 joint, due to a lack of $ZrSiO_4$-to-Si_3N_4 bonding. Joint strengths as high as 175 MPa were obtained with the ZrO_2 interlayer.

Mecartney, Sinclair and Loehman (16) joined hot-pressed Si_3N_4 using an MgO-Al_2O_3-SiO_2 glass composition as a joining material. Composition of joining material was chosen to approximate the oxide portion of the grain-boundary phase in the Si_3N_4. Joining was accomplished by furnace heating the materials to 1550 - 1650 °C. Findings focused on the kinetics of the reactions between Si_3N_4 and the joining material. The driving force for the joining was linked to lowering of Si_3N_4 interfacial energy when it is wet by molten silicate. In further research on this joining system, Johnson and Rowcliffe (17) examined the joining of hot-pressed Si_3N_4 using this oxide glass with an approximate composition of (in wt%): 55 SiO_2, 35 MgO, and 10 Al_2O_3. The joining technique involved a glazing step, followed by a pressureless reaction treatment of 30 to 60 minutes at 1575-1650 °C. Dissolution of the Si_3N_4 and growth of Si_2N_2O crystals into the joint were reported. The strength of joined test bars was found to be dependent on joint thickness, with an optimum joint thickness between 20 and 40 μm. A maximum room temperature strength of 460 MPa was achieved.

Iwamoto, Umesaki, and Haibara (18) successfully joined hot-pressed Si_3N_4 using a CaO-SiO_2-TiO_2 glass interlayer without applied pressure. A nearly eutectic glass composition was selected for the joining agent. The average CTE for the glass composition used was measured as 1.29×10^{-6}/°C (from 23 to 628 °C). Joining was accomplished by furnace heating the materials between 1400 and 1600 °C in a N_2 atmosphere. Reactions between the Si_3N_4 and the glass were studied in detail. Relatively high room temperature bond strengths of over 300 MPa were reported and put to practical use in the fabrication of curtains for the hot blast stove used in steel making.

Increased bond strengths were observed with the addition of α- Si_3N_4 powder to the glass joining agent.

Okida *et al.* (*19*) successfully joined Si_3N_4 using a CaF_2/kaolinite mixture (70/30 wt %) as a joining agent. Joining was accomplished by Joule heating, as opposed to furnace heating. Optimum electrical joining conditions were determined using this joining agent. Their study focused on reactions between CaF_2 agent and the Si_3N_4 substrate, analysis of the joint layer, and comparison of the strength of the joint compared to a joint obtained via furnace heating using the same agent. Results indicated that joining was accomplished by the formation of reaction zones and diffusion of the components in the joining agent and the sintering aids in the Si_3N_4. The joint layer was composed of a glassy substance consisting of Ca-Al-Si-Y-O-(F)-(N) (with F and N being minor elements) and contained a few particles of β-Si_3N_4. The reduced quantity of F was the result of a series of complicated evaporation reactions. Joined bodies were obtained with strengths of about 300 MPa up to 800 °C . Results also indicated that joints obtained via electrical joining were superior to those produced with this agent in the furnace.

In O'Brien's study (*20*) conducted for the US Department of the Interior's Bureau of Mines, commercial Si_3N_4 pieces were joined using numerous oxynitride glasses. Thirty glass compositions in the Y-Si-Al-O-N system were studied as joining agents for three different types of commercial Si_3N_4 (sintered with Y_2O_3 and Al_2O_3 aides, hot-pressed with primarily Y_2O_3, and hot-pressed with MgO and Al_2O_3 aids). Three different procedures for applying the glass interlayer were analyzed: placement of a thin plate between the Si_3N_4 pieces and application high temperature, use of capillary forces to draw molten glass between two Si_3N_4 parts, and application of glass powder in an organic binder to the joint surface. The thin plate procedure proved the best due to its simplicity and reproducibility. Glass-filled joints were successfully used in the hot-

pressed Si_3N_4 pieces and were comparable in fast fracture strength to their unjoined counter-parts up to approximately 1000 °C. Above this temperature, strengths decreased rapidly and glass flow failure began.

Takeuchi et al. (21) used a paste of Y_2O_3-Al_2O_3-SiO_2 mixed powder to join Si_3N_4 pieces. This paste was applied to the Si_3N_4 base piece using screen printing, followed by binder burnout. Joining was carried out in a N_2 atmosphere for two hours at 1700 and 1800 °C, followed by HIPing at 1700 °C at 98 MPa for one hour. Room temperature and 1200 °C joint strengths after pressureless sintering alone were measured at 250 and 160 MPa, respectively. HIP processing achieved room temperature and 1200 °C strengths of 620 and 370 MPa, respectively. This increase in strength was attributed to the fact that fractures ran through both the interface and the base Si_3N_4 material.

Walls and Ueki (22) joined low-z β-SiAlON ceramics (with the stoichiometric formula $Si_{(6-z)}Al_zO_zN_{(8-z)}$ and $z = 0.2$ in this study) using β-SiAlON-glass forming adhesives consisting of ground Si_3N_4, Y_2O_3, Al_2O_3, and SiO_2 powders. A β-SiAlON:glass ratio of 60:40 gave an optimum joint strength of 650 MPa in four-point bending when joining was carried out at 1600 °C for 10 min under an applied uni-axial pressure of 2 MPa. Bonding pressures in excess of 2 MPa caused excessive compression creep distortion during joining. Data from the study also indicated that hot isostatic pressing reduces the size of critical defects in the joint and improves the fracture toughness of the joint.

Use of oxide glass systems for joining Si_3N_4 is promising for low temperature applications, with room temperature strengths as high as 85% that of unbonded Si_3N_4 attained (22). However, high temperature joint strengths of this magnitude have not been demonstrated. One reason for this is the CTE mismatch between the glass and the Si_3N_4. In the work by Iwamoto, Umesaki, and Haibara (18), the CTE of the glass averaged about

1/3 that of Si_3N_4 and compressive stress between the Si_3N_4 and the glass was produced. In the system studied by Johnson and Rowcliffe (*17*), the CTE of the glass used was almost double that of hot-pressed Si_3N_4 and tensile stresses between the glass and the Si_3N_4 were produced. Another reason for insufficient high temperature strengths using glass interlayers is that a glass with a low T_g will soften and fail at too low a temperature. A glass system is desired which offers thermal stability and a closer CTE match across the ceramic-glass interface.

2.2 Celsian Glass Research

One advantage of using a SiO_2-SrO-Al_2O_3-based glass system is its ability to crystallize into monoclinic celsian. Celsian has a high melting point and a CTE of $2.29 \times 10^{-6}/\,°C$ (from 20 °C to 1,000 °C), very close to that of hot-pressed Si_3N_4. An important aspect of using a celsian-based composition is controlling the sluggish phase transformation reaction between monoclinic celsian and hexacelsian in the (Sr)-(Ba)O-Al_2O_3-$2SiO_2$ system. This hexacelsian phase forms metastably in celsian glass at all temperatures including those below 1590 °C, the temperature for transformation (see figure 1). To complicate matters more, a rapid and reversible transition from hexacelsian to an orthorhomic hexacelsian is observed at 300 °C, which is accompanied by a volume change (approximately 3-4 %). A ternary equilibrium phase diagram for the BaO-Al_2O_3-SiO_2 system, depicting the relationship between celsian and hexacelsian phases, is presented in figure 1.
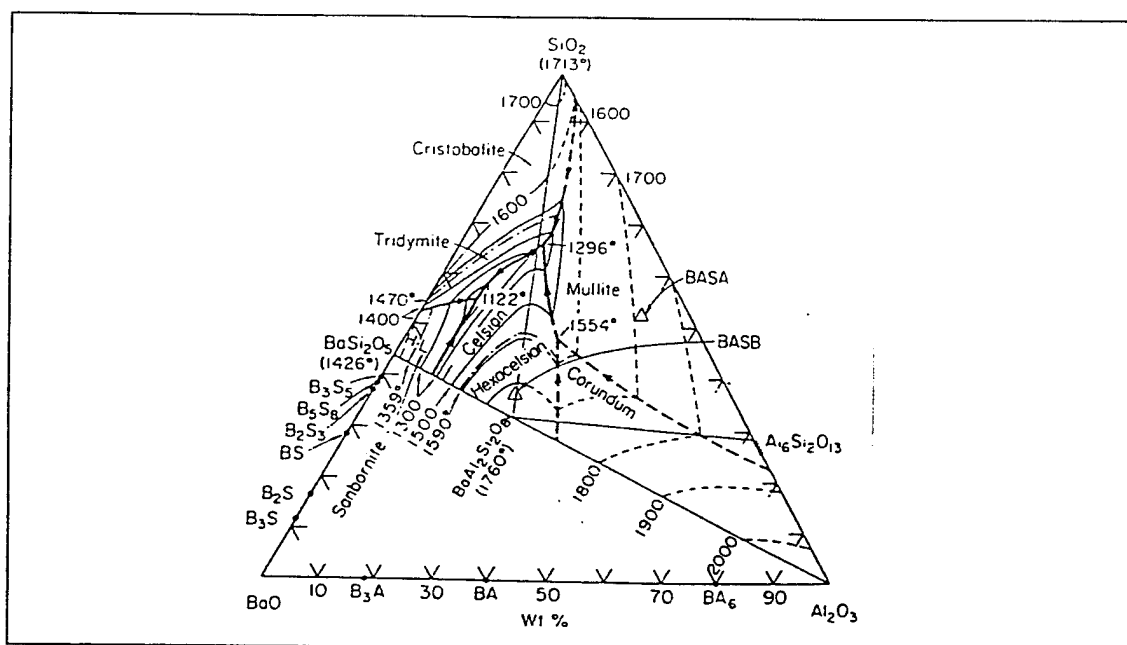
Fig. 1 BaO-Al₂O₃-SiO₂ Ternary Phase Diagram (24)

Bansal and Hyatt (25) studied (Sr, Ba)O-Al₂O₃-2SiO₂ glasses of various compositions to determine the effect of the presence of SrO in BaO-Al₂O₃-2SiO₂ glass on physical properties. Densities, flexural strengths, linear thermal expansion, glass transition temperatures and crystallization temperatures were determined for each composition. The liquidus and crystallization temperatures from the melt were also measured. Crystalline phases that formed on heat treatment were identified by powder X-ray diffraction. In Sr-containing glasses, the monoclinic celsian phase always crystallized at temperatures above 1000 °C; at lower temperatures the hexagonal analogue formed. The temperature for orthorhombic-to-hexagonal structural transformation increased with SrO content.

Drummond III et al. (26) investigated the crystallization of a celsian glass composition (barium-aluminosilicate) as a possible high-temperature ceramic matrix material.

Although this research dealt exclusively with barium-based celsian, the results are important in terms of the data on the hexacelsian to celsian transformation. Heat treatments (up to 1290 °C) of the glass composition resulted in crystallization of the hexacelsian phase unless a flux, such as Li_2O was added or a nucleating agent was used. Glasses with Mo additions contained hexacelsian, mullite, and Mo-rich glass. Li_2O additions stabilized the celsian phase, but mullite and Mo-rich glass were still present.

Bansal and Drummond III (27) studied the kinetics of hexacelsian-to-celsian phase transformation. Phase-pure hexacelsian was prepared by heat treatment of glass flakes at 990 °C for 10 hours. These flakes were then isothermally heat treated at different temperatures in a range between 1,000 °C and 1,200 °C for various times. The amounts of monoclinic celsian formed were determined via quantitative X-ray diffraction. Values of the reaction rate constant (k) were determined at various temperatures from the Avrami equation:

$$x = 1 - \exp[-(kt)^n]$$

where x is the volume fraction transformed after time t, k is the reaction rate constant, and n is the Avrami exponent. The Avrami parameter (n) was determined to be 1.1. From the temperature dependence of k, the apparent activation energy for this transformation reaction was evaluated to be 527 ± 50 kJ/mol (126 ± 12 kcal/mol).

Barbieri et al. (28) explored the capability to sinter surface-nucleated barium and strontium feldspar ($(Ba-Sr)O-Al_2O_3-SiO_2$) glass ceramics. Sintering was concluded to be very useful for the production of low porosity (less than 3 vol %) materials that were greater than 95 % of theoretical density, and the favored formation of thermally stable celsian and Sr-celsian. Compared to bulk crystallization, sintering of surface-nucleated particles reduces the formation of hexacelsian in favor of the monoclinic celsian phase. Microhardness values of 470 - 780 Kg/mm^2 and elastic modulus of 57 - 115 GPa of the

sintered glass-ceramics, together with the refractories of the developed phases, make the systems very suitable for structural applications.

2.3 Overview

Braze metal interlayers and oxide glass systems previously studied have not demonstrated the capability to achieve sufficiently strong, high temperature Si_3N_4 joints (between 200 and 250 MPa (at 1200 °C) for Al-based joints and up to 370 MPa (at 1200 °C) for oxide glass-joined materials. The main reasons for these relatively low strengths compared with room temperature results lie in the very low CTE of hot-pressed Si_3N_4 and the low melting and softening temperatures of ductile interlayers. Furthermore, although solid state diffusion bonding of Si_3N_4 components at high pressure and temperature eliminates this mismatch, the technique is limited in terms of the shapes that can be formed. What is needed to form complex shapes from Si_3N_4 is a joining technique with high temperature strength, such as can be achieved with a glass system with a closer CTE match and greater thermal stability. Since celsian glass offers these advantages, it should provide a promising joining system.

3 EXPERIMENTAL PROCEDURE

3.1 Preparation and Analysis of Materials

A single type of commercial Si_3N_4 and two different glass compositions were used in this research. A commercial hot-pressed $Si_3N_4^*$ was used because it is readily available and has acceptable properties. Glass compositions were varied by increasing the amount of Al_2O_3 while maintaining a constant SiO_2:SrO ratio of 54:46 wt %.

3.1.1 Commercial Si_3N_4

Commercial, hot-pressed Si_3N_4 containing Y_2O_3 and Al_2O_3 densification aides was used. Data provided by the manufacturer for this Si_3N_4 are listed in Table 2.

Table 2 Si_3N_4 Material Properties**

Property	Units	Value
Density	kg/dm^3	3.3
Open Porosity	%	0
Flexural Strength @ 20 °C	MPa	850
Thermal Conductivity @ 20 °C	W/m K	18
Thermal Expansion Coefficient 20-1000 °C	$\times 10^{-6}/$ °C	3.3
Thermal Shock Resistance	ΔT (°C)	>600
Specific Heat	J/kg K	800
Maximum Use Temperature	°C	1100

** Provided by manufacturer

---

* Morgan Matroc Limited
  Bewdley Road Stourport-on-Severn
  Worcestershire DY13 8QR England

3.1.2 Grain Boundary Characterization

Analysis of the Si_3N_4 grain boundary composition was accomplished by electron microprobe analysis. A Japan Electron Optics Laboratory (JEOL) JXA-8600 electron microprobe X-ray analyzer using a wavelength dispersive spectrometer was used for the analysis. An accelerating voltage of 15 keV and a current of 25.02 nA were employed. A one micron point scan with one micron steps was traced across several grain boundaries in the Si_3N_4 substrate. Graphical analysis was accomplished using a Versaterm Pro data conversion program to convert the raw data to a spreadsheet.

3.1.3 Silicate Glass Preparation

SiO_2, SrO, and Al_2O_3 powders were used to make the glass compositions. Purities for these powders were 99.5%, 99.5%, and 99.9+% for the SiO_2, SrO (metals basis), and Al_2O_3 (metals basis), respectively. Two glass compositions were prepared by dry mixing in a ball mill for one hour using lucite mixing balls. Compositional data for these glass samples are presented in Table 3.

Table 3 Glass Compositions

Sample	SiO_2:SrO:Al_2O_3 (wt%)	SiO_2:SrO:Al_2O_3 (mol %)
SAS-5	51:44:5	64:32:4
SAS-10	49:41:10	62:31:7

After mixing, samples were pressed under an applied load of one metric ton using a hydraulic press. The samples were furnace-heated to 1600 °C in air in a Pt crucible and quenched in room temperature water. After removal from the crucible, glass batches designated for use in wetting experiments were placed in Pt foil and reheated to 1600 °C and cooled to room temperature. These glass melts were then annealed at 1000 °C in air

and furnace cooled. The Pt foil was peeled away and the glass was examined under polarized light for visible stress lines. Glass samples not designated for use in wetting experiments were ground to 150 μm powder using an iron mortar.

3.1.4 Glass Characterization

The coefficient of thermal expansion (CTE) for each glass composition was measured to the softening point on a Netzsch differential, double-pushrod dilatometer using sintered Al_2O_3 as a standard. Simultaneous heating of the sample and the reference was accomplished in air in an electrically heated furnace at a rate of 20 °C/min. Quartz glass scanning rods were used to pick up the dilation of the sample and the Al_2O_3 reference. CTE measurement was accomplished on glass samples that had been annealed and manufactured into billets comparable in size to the reference specimen. The glass transition temperature (T_g) values for each glass composition were also derived from dilatometer results. T_g and the temperature of the onset of the first crystallization exotherm (T_c) were measured using a differential thermal analysis (DTA) -1600 apparatus. DTA was accomplished on glass samples ground to 150 μm particle size. DTA was conducted using Pt crucibles in an Ar atmosphere and Al_2O_3 as a standard with a heating rate of 20 °C/min.

3.1.5 Glass Crystallization Experiments

Crystallization experiments on the glass compositions were approached by furnace heating the glass particles in air using Pt foil. Heat treatment profiles were determined using DTA results that indicated the onset of the crystallization exotherm for each composition. Following heat treatment, samples were furnace cooled to room temperature and the specimens were removed from the Pt foil. Small pieces were detached and ground to 50 μm particle size for XRD analysis. A Siemens D500 diffractometer with a copper anode, 40 kV voltage, 30 mA tube current, and a K-α filter

was employed, with settings based on 2θ stepped from 10 to 60° in 0.05° increments.

3.2 Contact Angle Experiments

Sessile drop experiments were conducted in a N_2 atmosphere in a resistance-heated

Materials Research Furnace (see figure 2) powered by a 30 kVA three phase main step
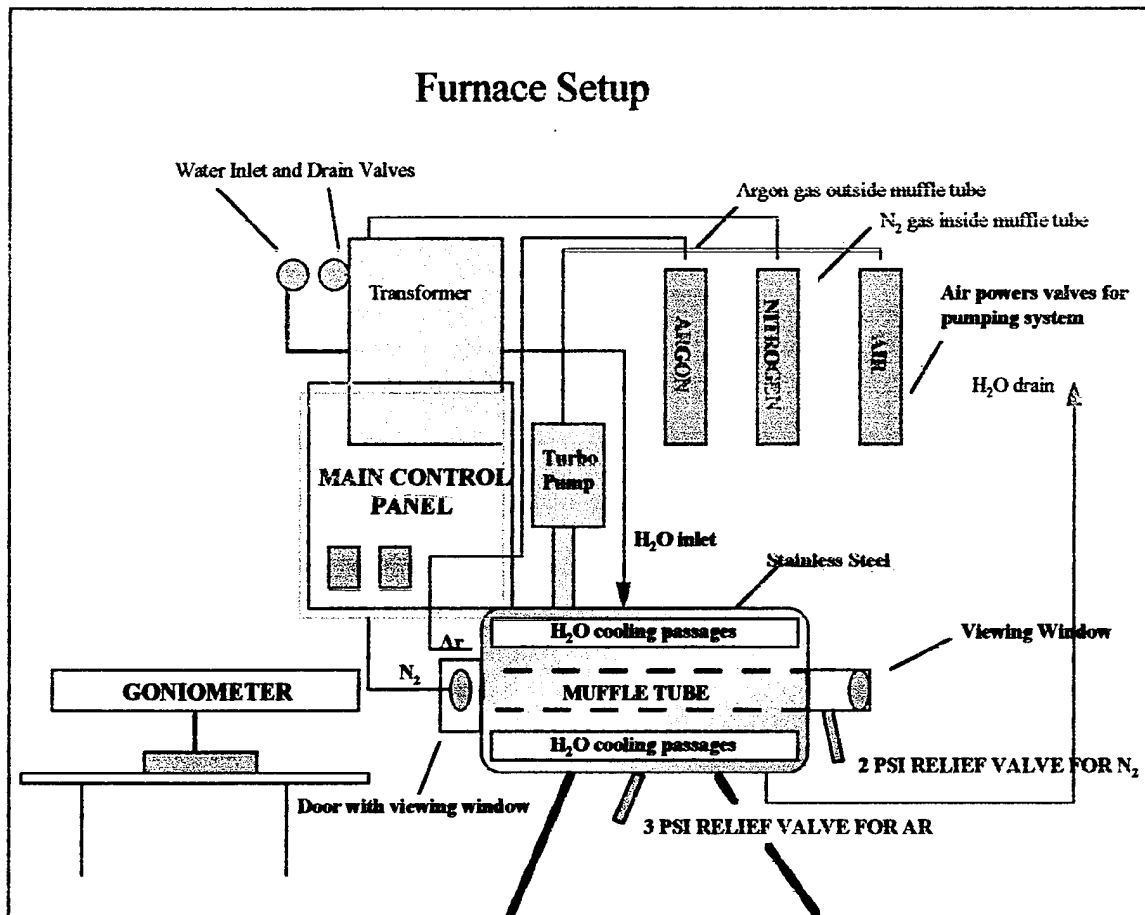
down transformer.

Fig. 2 MRF Setup for Contact Angle Measurement and Wetting Experiments

The furnace was equipped with a graphite heating element, a 24 inch long alumina muffle

tube (inside and outside diameters of 2.25 and 2.5 inches, respectively), and a graphite D-

tube for sample placement. The temperature was controlled by a Honeywell UDC-5000

temperature programmer controller. A turbo-pumping system was employed to purge the muffle tube after sample loading and after sample removal (for storage purposes). This vacuum system consisted of a Leybold TMP-361 turbo pump, a VRC electro-pneumatic large port high vacuum valve, a Leybold Tri-Vac rotary vane dual stage mechanical pump with inlet and exhaust filters, and an Allen-Bradley SLC-500 programmable controller to control pumping system logic. Temperature monitoring above and below the muffle tube was accomplished by two 1/8 inch diameter type 'C' tungsten/rhenium thermocouples, calibrated via 5 wt% Re vs. 26 wt% Re. The thermocouples were sheathed by eight inch long by 0.02 inch diameter molybdenum sheaths and each used 30 AWG thermocouple wire gauge and BeO insulation.

3.2.1 Determination of Temperature Range for Wetting

Specimens of SAS-5 and SAS-10 glass were made into small cubes with dimensions between 2 and 4 mm. The cubes were placed on Si_3N_4 plates cut into dimensions of $11 \times 11 \times 5$ mm and ground to a 600 grit finish. The glass cube/Si_3N_4 assemblies were heated for various times, depending on the composition of the glass, at temperatures between 1350 °C and 1550 °C under a N_2 atmosphere. For each composition, the first sessile drop experiment was designed to determine the upper and lower temperature limits for wetting. The lower limit was the temperature at which wetting began (i.e. when the contact angle between the molten ball of glass and the substrate became acute; see figure 3). The upper temperature limit was designated as the temperature at which gas bubbles began to escape from the molten glass due to the dissociation of $SiO_{2(l)}$ into $SiO_{(g)}$ and $O_{(g)}$. Contact angles were measured using a Ramé-Hart telegoniometer, with maximum magnification of 25× at a working distance of 1200 mm, positioned to view the center of the heat zone in the muffle tube (see figure 2).
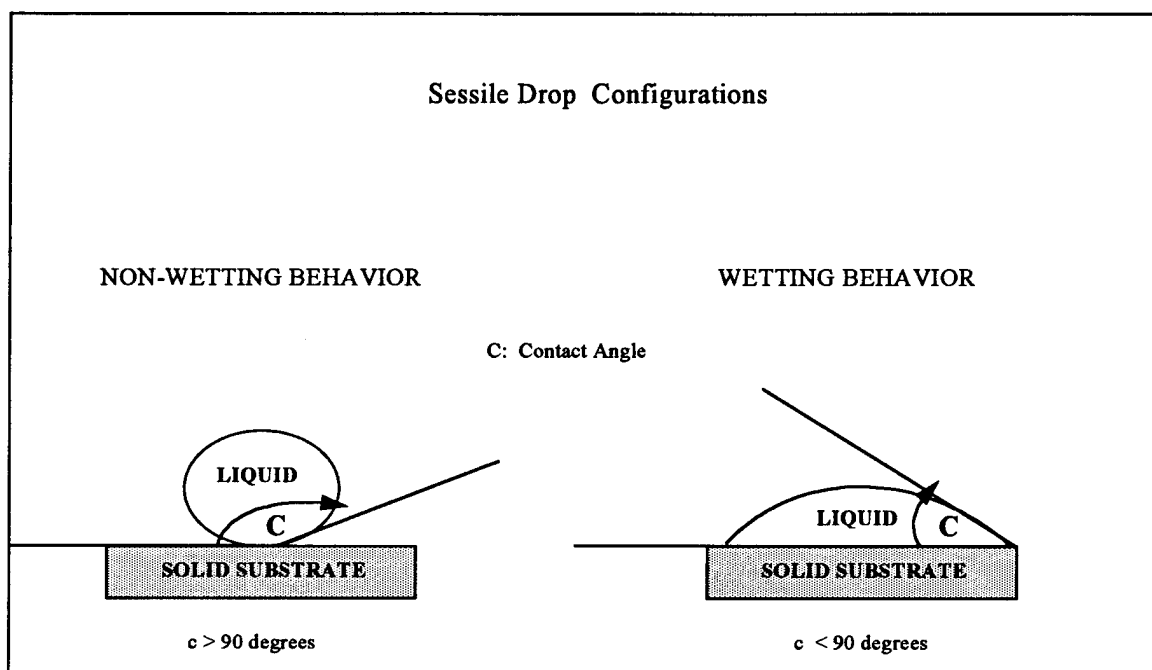
Fig. 3 Contact Angles and Wetting Behavior (adapted from *Ref 29*)

3.2.2 Wetting Analysis

After determining the temperature range for effective wetting, a series of wetting experiments using a matrix of temperature and time parameters was designed for each glass composition. Three temperatures (50 °C apart) within the wetting range, and three duration profiles (7.5, 15, and 30 min) were utilized for each composition. Heat treatments consisted of heating at 30 °C/min up to 1250 °C (holding 5 min), heating at 5 °C/min to the specified wetting temperature (holding for specified duration profile), and furnace cooling to room temperature. The average rate of furnace cooling was approximately 40 °C/min.

3.2.3 Contact Angle Measurement

Contact angle measurements were carried out for each glass composition by heating at 30 °C/min up to 1250 °C (holding 5 min), and then heating at 5 °C/min to 1325 °C, a temperature in the lower end of the wetting range spectrum for each composition (holding

indefinitely until the contact angle diminished or reached steady-state). Contact angles were measured using the telegoniometer described above. Measurements were taken at constant temperature and at one minute intervals on both sides of the substrate.

3.3 Electron Microprobe Analysis of the Diffusion Zone

The cooled glass/substrate samples treated in the furnace were potted in epoxy resin and sectioned perpendicular to the interface using a low-speed diamond saw. The samples were then ground, polished and coated with approximately 200 Å of carbon to make the sample electrically conductive so as to prevent charging of the sample. Electron microprobe scans were used to analyze the interdiffusion of the glass and grain boundary phase in the Si_3N_4. Quantitative analysis of the composition of the wetted region was measured using a JEOL scanning electron microprobe (see 3.1.3 for more details on microprobe configuration, voltage, and current). Twenty μm long line scans with a 1 μm beam were oriented parallel to the interface and were stepped from the substrate into the melted glass in 2 μm steps. The line scans started outside the diffusion zone in the Si_3N_4 and went into the glass as far as possible (until encountering a crack in the glass). Analytical raw data were automatically corrected for instrumental effects. Matrix effects were handled by the Bence-Albee oxide analysis routine correction procedure (*30*). This routine ignored nitrogen and assumed oxygen to be present in the usual stoichiometric ratios. The reason for using this routine is that nitrogen x-rays are preferentially absorbed by carbon in the chamber. Carbon is used to coat the sample; carbon is part of the atmosphere inside the probe (because of the hydrocarbons from the oils used in both the diffusion and roughing pumping systems); and carbon is the major element in the windows of the x-ray detectors. Use of this procedure, however, results in problems with calculating the concentrations of Si, since all Si is taken to be present in the form of SiO_2, instead of Si_3N_4. This problem is of only minor importance since the focus of the diffusion analysis is on the other oxides in the glass and Si_3N_4 grain boundary.

3.4 SEM Analysis of the Diffusion Zone

Secondary electron micrographs and back-scattered electron images were used to obtain qualitative documentation of the diffusion zones in the melted glass/substrate samples. Elemental distribution photomicrographs employing Y, Al, Si, and Sr elemental maps were used to obtain semi-quantitative diffusion analysis for the varying ionic concentrations across the interface.

3.5 XRD Analysis of Diffusion Zone

Additional analysis of the diffusion zone resulting from the wetting was accomplished by XRD analysis (see 3.3 for XRD configuration). For this analysis, separate wetting experiments were conducted at two different temperatures in the wetting range using the SAS-5 composition and at an elevated temperature using the SAS-10 composition. The excess molten glass on top of the substrate was removed by grinding with 600 grit SiC grinding paper, leaving a very thin layer of reacted glass of approximately 50 μm thickness. The specimen was then analyzed using XRD to determine the presence of any crystalline phases. A grazing incident angle XRD method was employed to focus on the reaction zone. This method utilized a grazing angle of 2° with 2θ stepped from 10 to 60° in 0.02 ° increments.

3.6 Joining and Strength Testing of Si_3N_4 Plates

Si_3N_4 plates were joined in a batch furnace using cleaned Si_3N_4 plates and applying SAS-5 and SAS-10 glass powder as a joining agent. Four-point bending tests were conducted on machined test bars at room temperature.

3.6.1 Si_3N_4 Preparation.

Si_3N_4 plates were machined into 22×45×5 mm pieces and ground and polished. The plates were then cleaned using a four-step cleaning procedure as follows. They were first

cleaned ultrasonically in 1,1,1,-Trichloroethane for two minutes (and rinsed) to remove

oils and other organic contamination. They were then ultrasonically cleaned in Span 80

detergent solution for two minutes (and rinsed in deionized water) to remove polar

materials and inorganic salts and particulate matter. The plates were then cleaned in

deionized water for two minutes to remove traces of detergent solution. Finally, the

plates were cleaned ultrasonically in isopropyl alcohol for two minutes and dried under a

heat lamp to remove any residual water and alcohol.

3.6.2 Application of Glass Joining Agent

A small amount of glass powder (0.2 g), ground to 75 μm particle size, was applied

evenly to the long side of one Si_3N_4 plate (45 mm side) using each glass composition.

This plate was then placed in a alumina/molybdenum fixture (see figure 4). Alumina

paper was positioned on either side of the Si_3N_4 plate to hold the glass powder in place.

Another Si_3N_4 plate was then placed on top of the glass powder in the secured fixture.
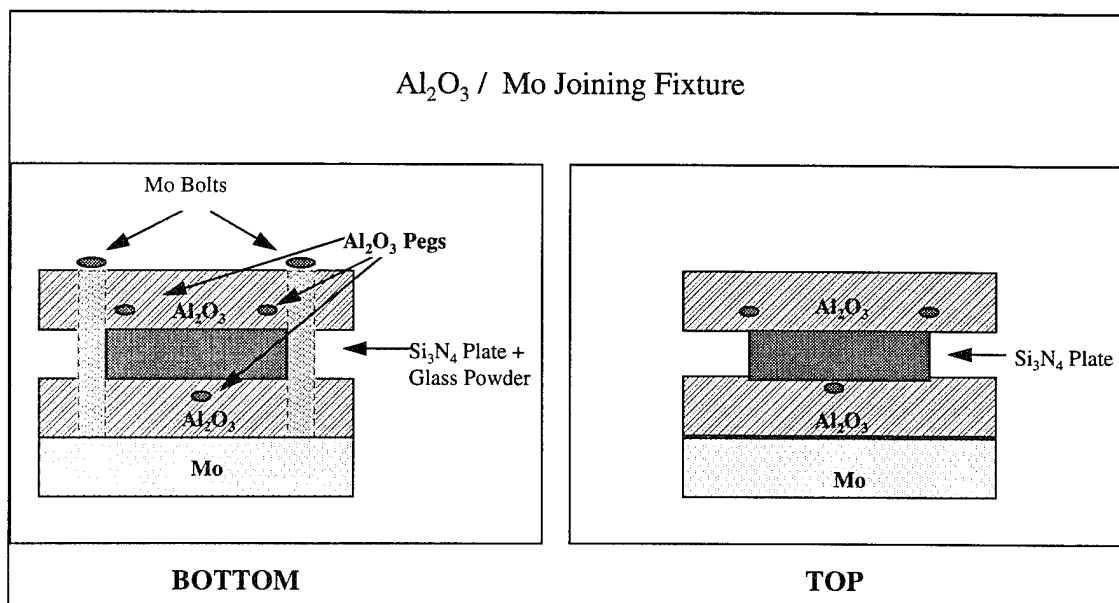
Fig. 4 Al_2O_3/Mb Fixture and Setup

3.6.3 Furnace Joining.

The Si_3N_4 and joint fixture was placed in an Astro Industries batch furnace (model number APF-0716-1800). For each glass composition, joining was carried out in a N_2 atmosphere at 1450 °C for 30 minutes (figure 5) using a ramp rate of 30 °C/min and furnace cooling. The approximate furnace cooling rate was 100 °C/min. These time and temperature parameters were selected based on wetting experiment and electron microprobe results. A 138 g. Mo weight was placed on top of the upper Si_3N_4 plate to achieve an applied load of 0.01 MPa.

Furnace Setup

N_2 Atmosphere

H_2O Cooled

Mo Weight

Si_3N_4 Plates
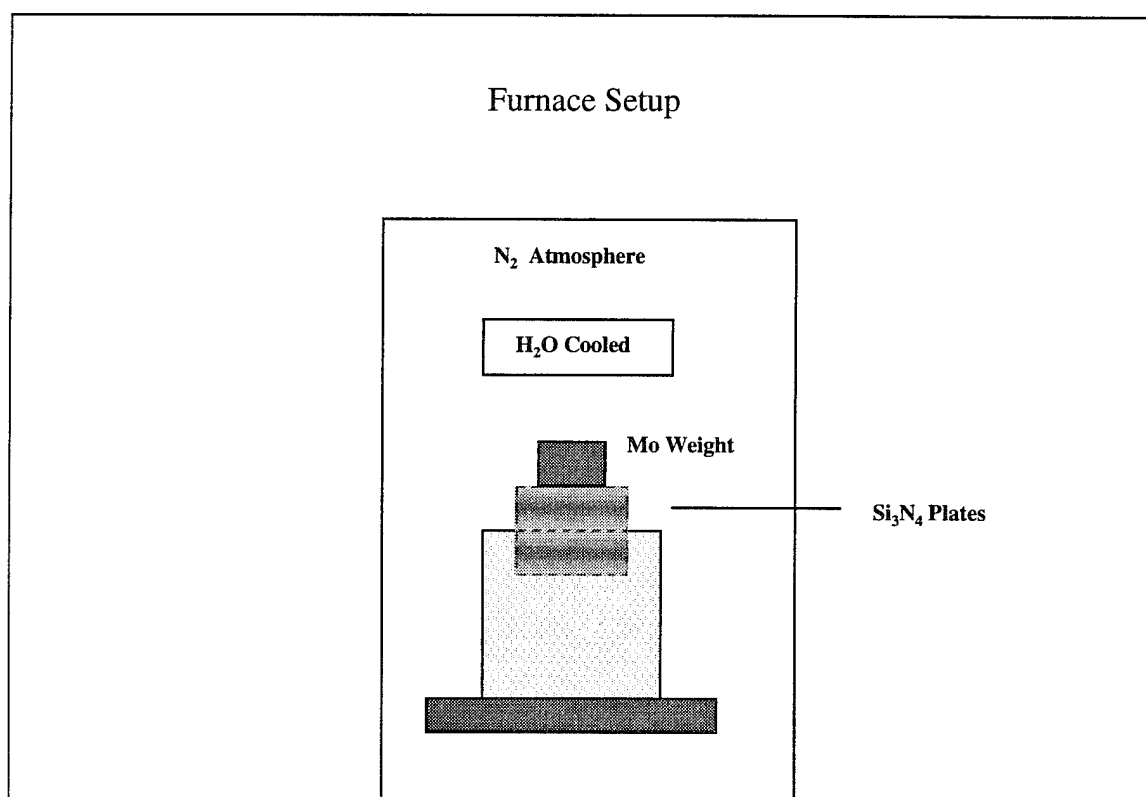
Fig. 5 Astro Batch Furnace Setup for Joining

3.6.4 Strength Testing

After joining, the joined Si_3N_4 pieces were sectioned perpendicular to the joint region into size B test bars IAW MIL-STD-1942A (*31*). These bars were then numbered sequentially to designate the distance from the center of the joined plates. Test bars were then subjected to four-point bending tests at room temperature using an Instron 5565 load frame.

4.1. Si₃N₄ Grain Boundary Analysis.

Electron microprobe analysis of the Si_3N_4 substrates revealed an overall, average

composition of approximately 5 wt% Al_2O_3 and 10 wt% Y_2O_3, with 85 wt% Si_3N_4.

Microprobe results are presented in figure 6 below. Fluctuations in concentration across

the substrate represent Si_3N_4 to grain boundary transitions. These fluctuations also

indicate the concentrations of Al_2O_3 and Y_2O_3 at the grain boundaries in the Si_3N_4.
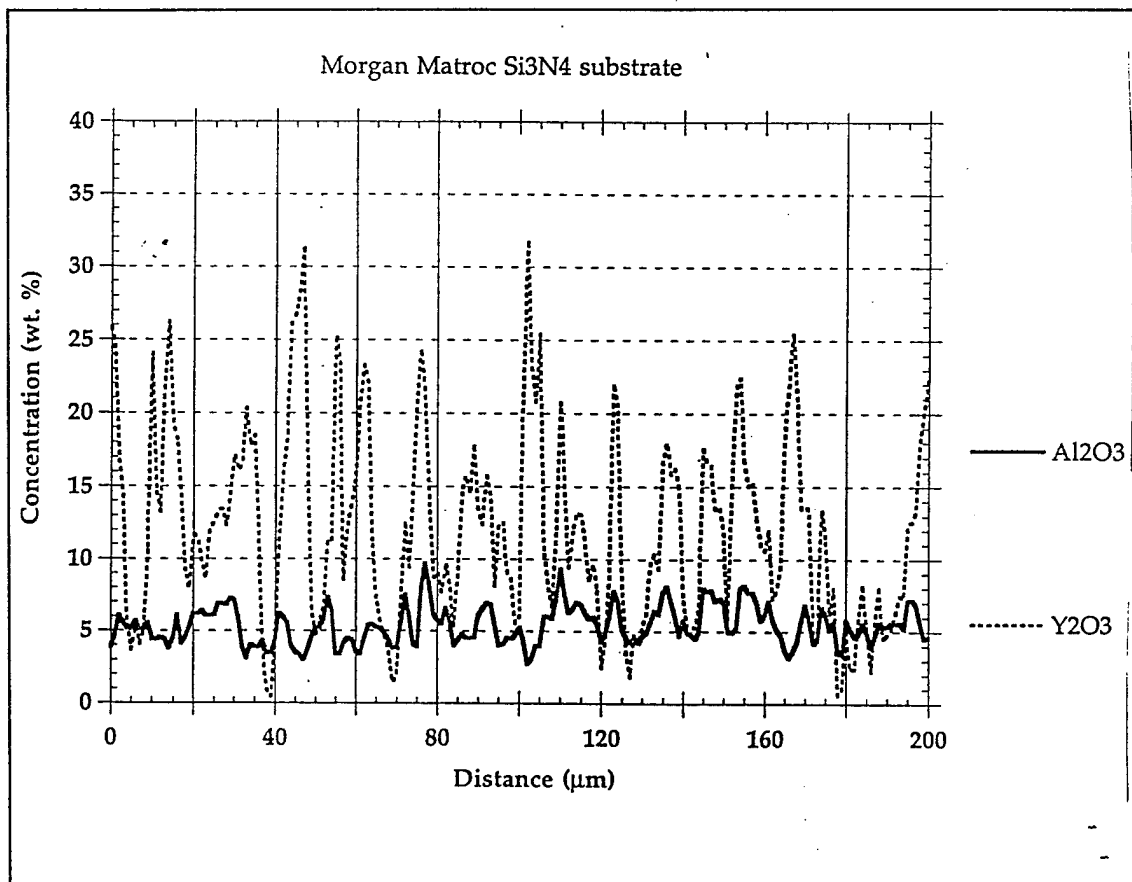
Fig. 6 Electron microprobe analysis of Si₃N₄ grain boundary composition. Microprobe scan taken in the bulk Si₃N₄ outside the diffusion zone in wetted Si₃N₄; distance starting point is arbitrary.

4.2 Glass DTA.

DTA results for the SAS-5 and SAS-10 glass compositions are presented in figures 7 and 8, respectively. These results reveal Tg values of 745 °C for SAS-5 and 770 °C for SAS-10. T_c values not quite as evident, but close analysis of the DTA plots, coupled with XRD results of crystallized samples, shows that these onset temperatures are approximately 1120 °C for SAS-5 and 1100 °C for SAS-10.
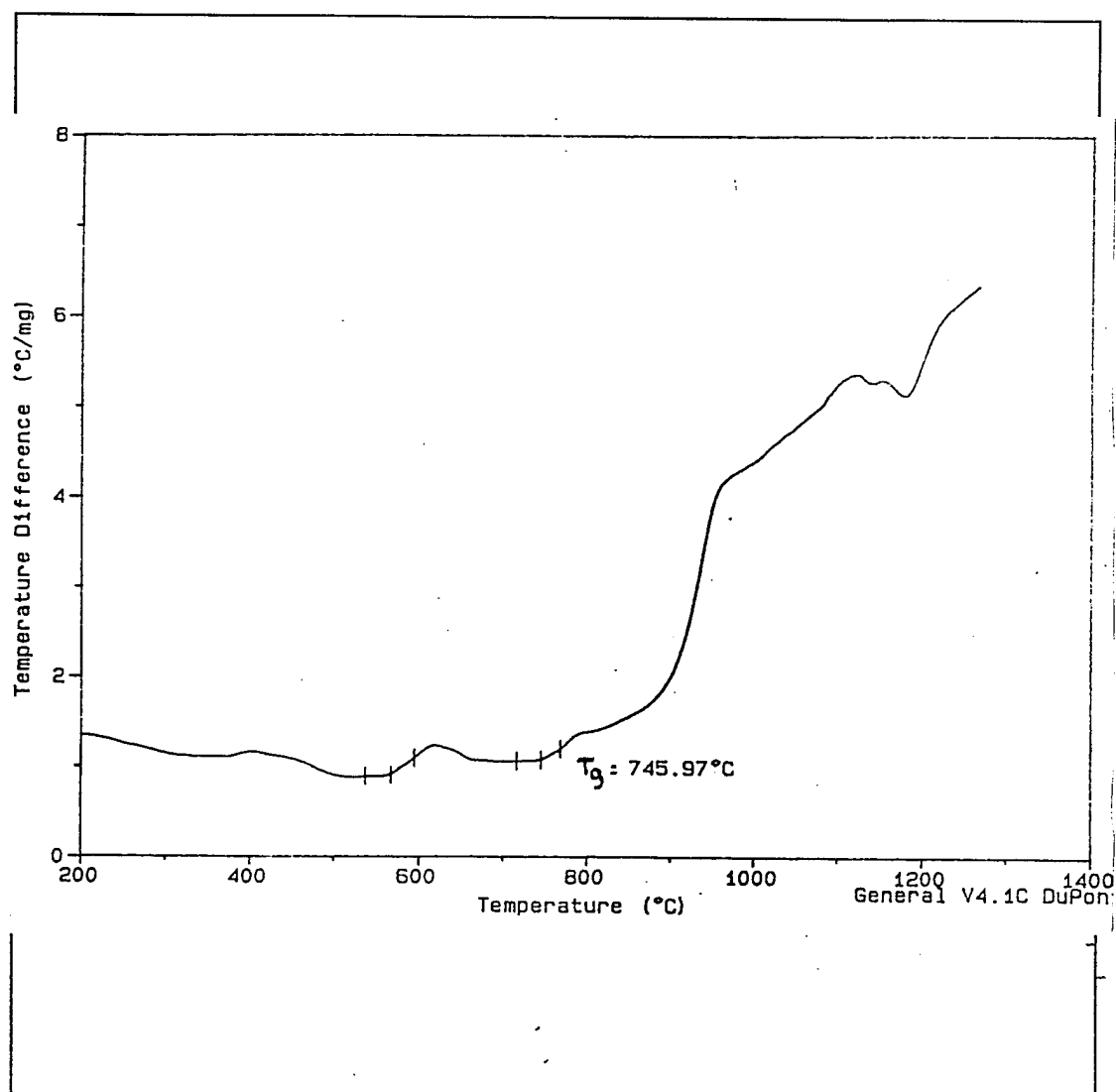
Fig. 7 DTA Plot for SAS-5 Composition
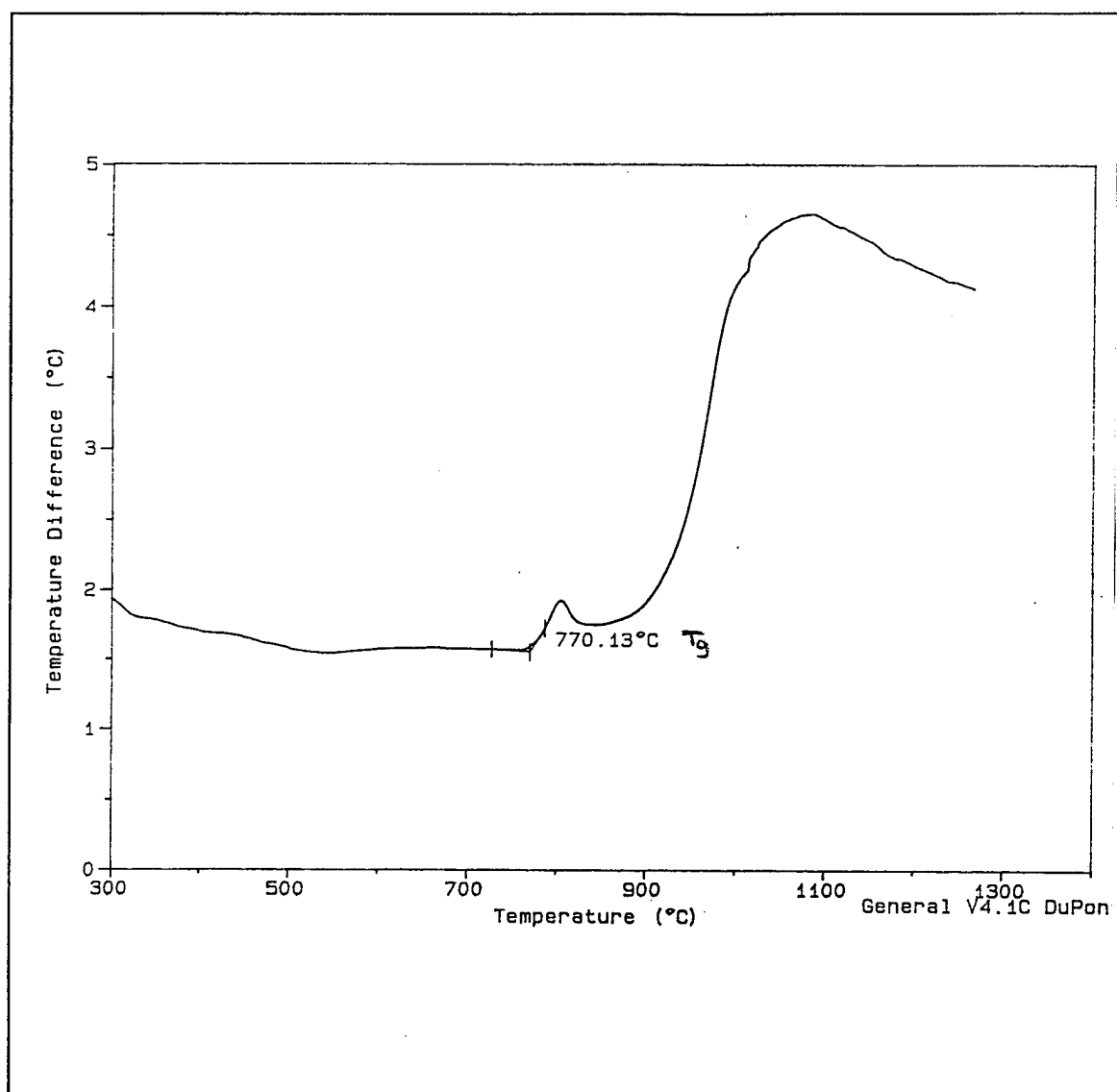
Fig. 8 DTA Plot for SAS-10 Composition

4.3 Glass CTE Measurement.

Dilatometer measurements for SAS-5 and SAS-10 samples are presented in figures 9 and 10, respectively. The CTE for each composition was measured as 8.54×10^{-6} /°C for SAS-5 and 8.46×10^{-6} /°C for SAS-10. T_g derivations from dilatometer measurements reveal T_g values for SAS-5 and SAS-10 as 740 °C and 774.8 °C, respectively.
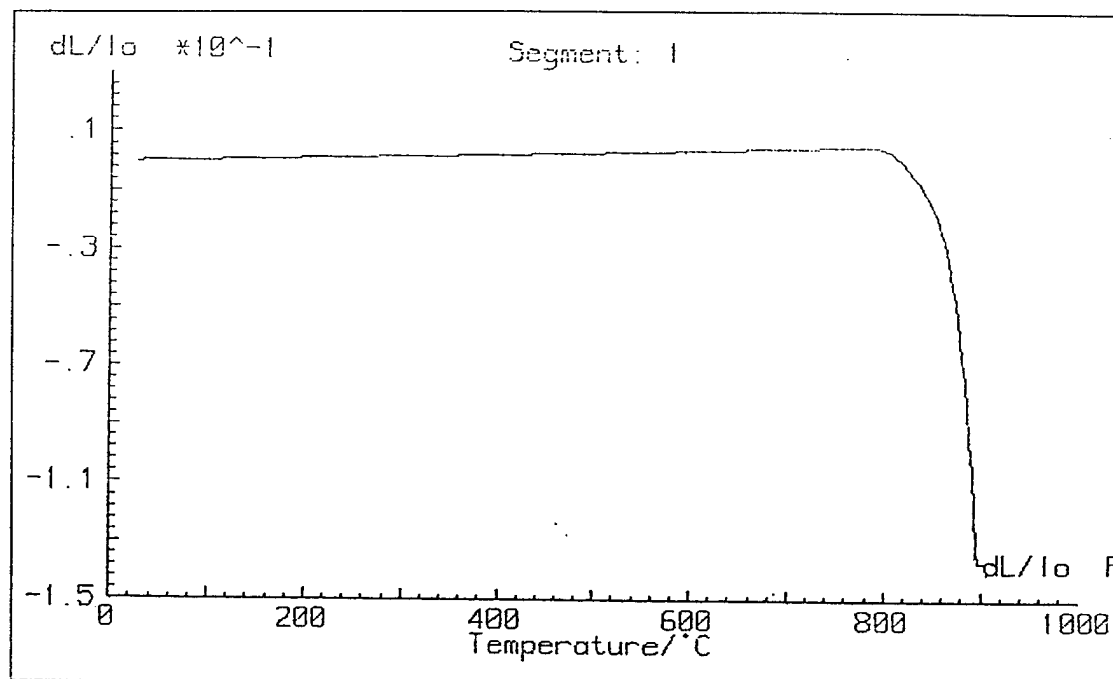
Fig. 9 Dilatometer Plot for SAS-5
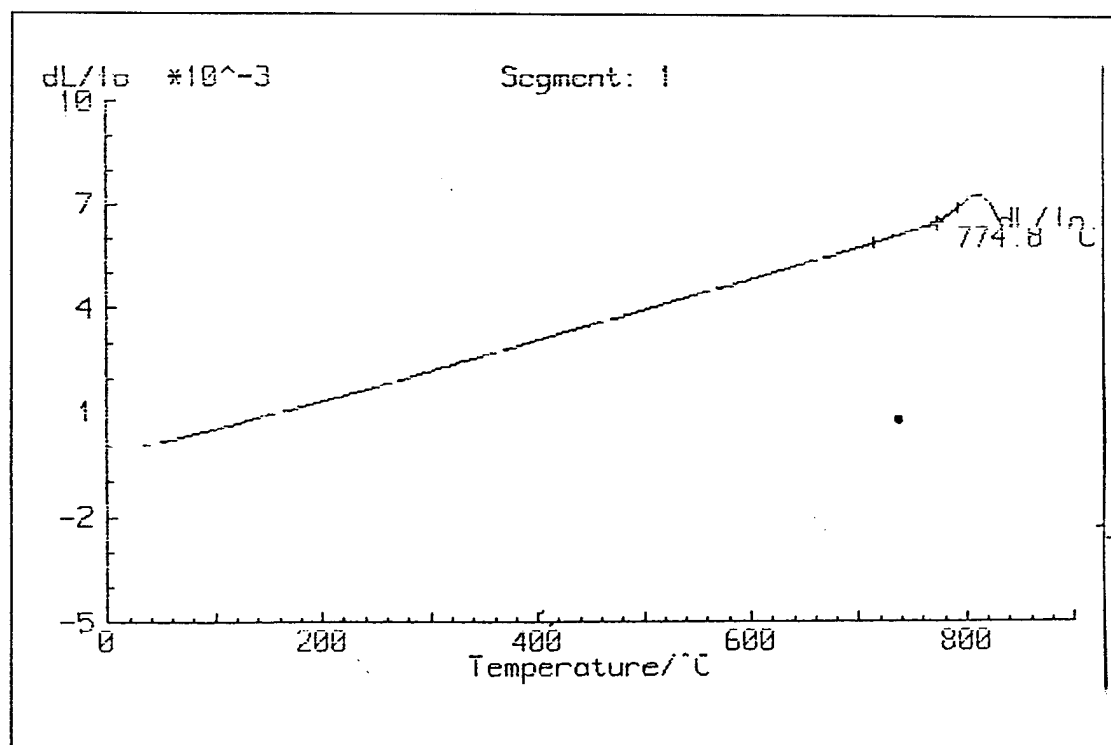
Fig. 10 Dilatometer Plot for SAS-10

4.4 Glass Crystallization Experiments.

Crystallization heat treatments for the glass compositions were based on DTA results presented in section 4.2. XRD analysis of SAS-5 glass pieces treated at 1000 °C for 30 minutes showed a completely amorphous (figure 11) phase. XRD analysis of SAS-5 heat treated at 1200 °C for 30 min revealed crystalline strontium-silicate ($SrSiO_3$, PDF# 34-0099) (see figure 12). XRD analysis of SAS-5 heat treated at 1000 °C for 5 hours, when ground to 50 μm powder, revealed no crystallinity. However, XRD analysis of this same sample, examined on the flat bottom of the specimen (which cooled slower than the rest of the sample), revealed crystalline strontium aluminum silicate ($SrAl_2Si_2O_8$, PDF# 38-1454) and other crystalline phases (figure 13). SAS-10 glass samples showed no evidence of crystallinity when heat treated for one hour at 1000 °C, 1150 °C, 1300 °C, 1500 °C, and 1550 °C; samples remained transparent. SAS-10 heat treated 1000 °C for 5 hours also remained transparent.

4.5 Wetting Experiments.

Results of wetting experiments for each glass composition can be summarized in two areas of investigation. The first area involves the temperature regimes for wetting behavior for each glass. The second area includes contact angle measurements made for each glass at constant temperature as a function of time.
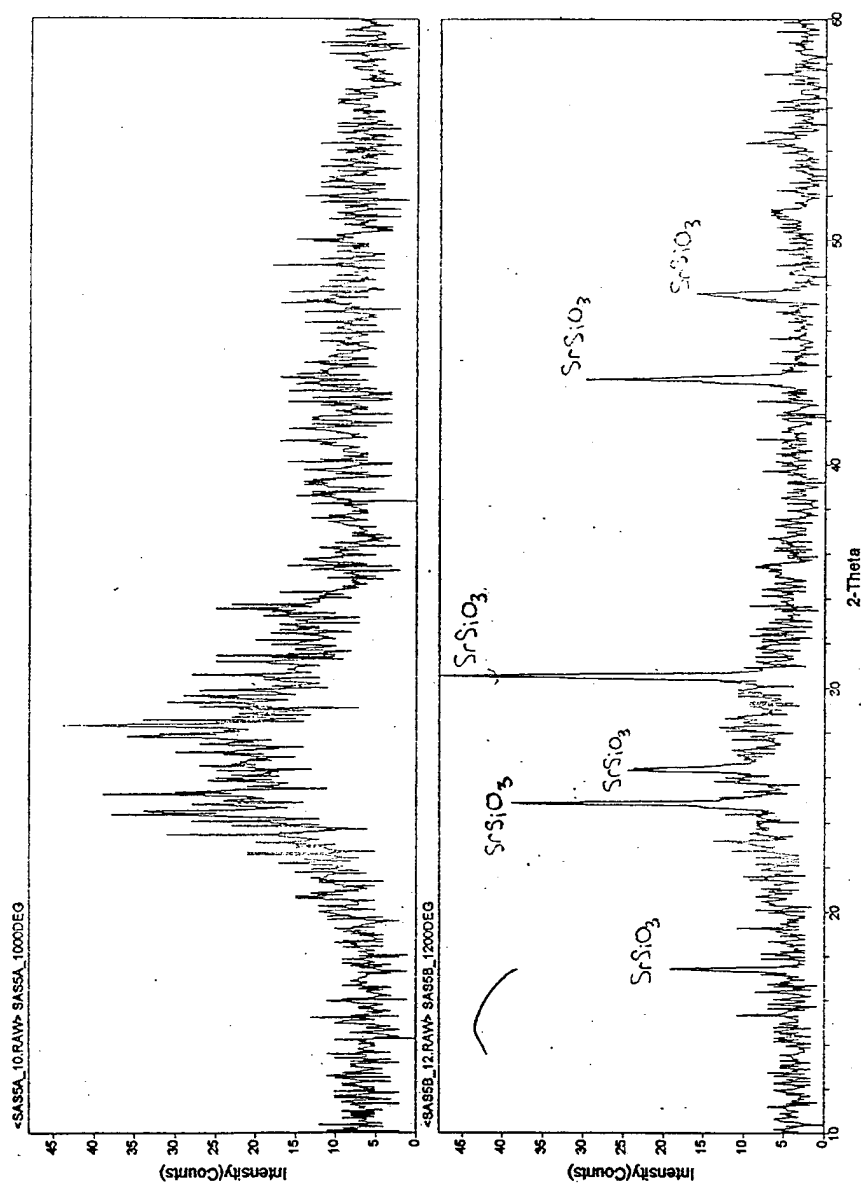
Fig. 11 XRD analysis of SAS-5 heat treated at 1000 °C for 30 min (top), showing sample to be completely amorphous; and SAS-5 heat treated at 1200 °C for 30 min (bottom) revealing the presence of strontium silicate ($SrSiO_3$) (PDF# 34-0099)
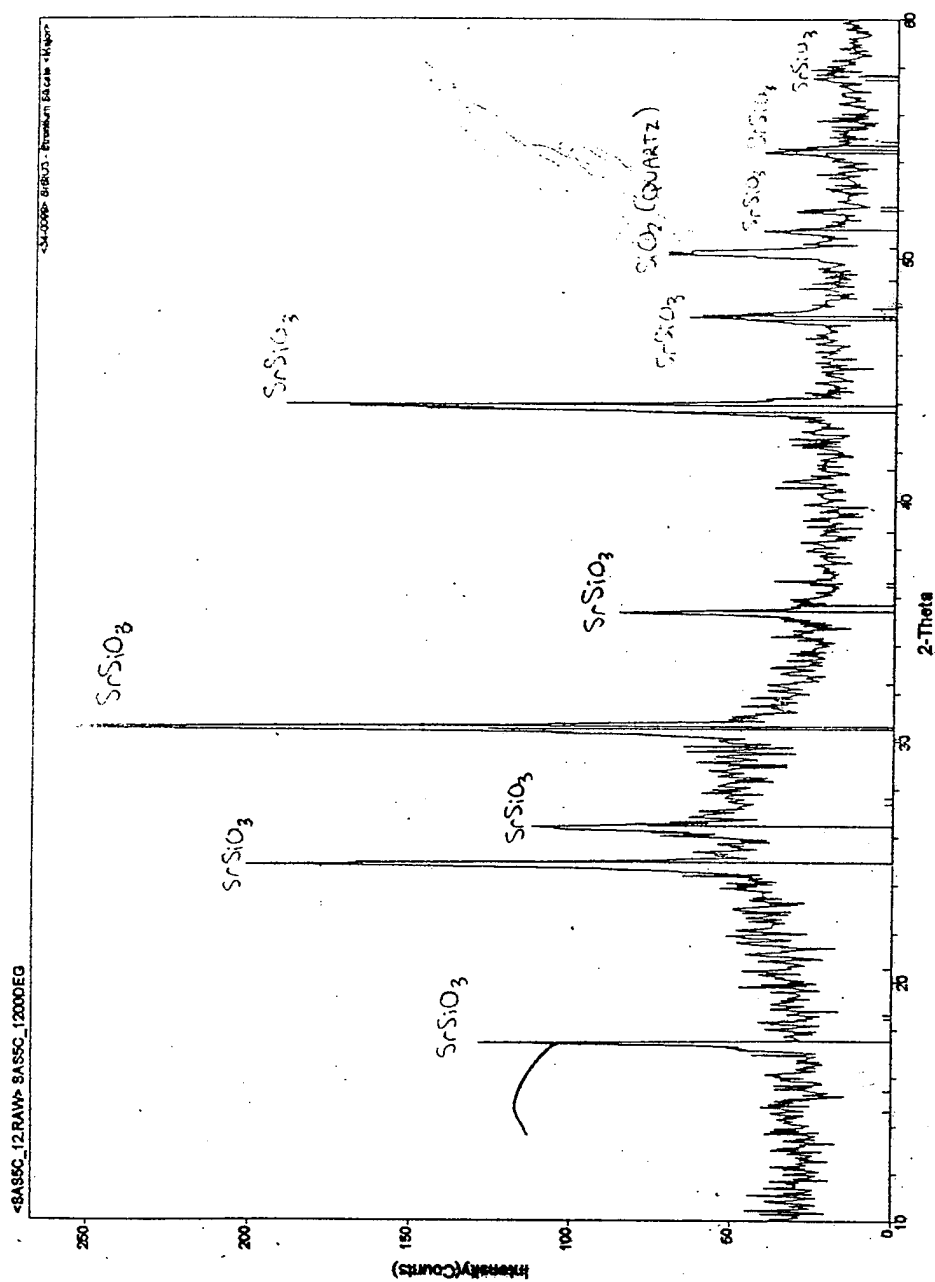
Fig. 12 XRD analysis of SAS-5 heat treated at 1200 °C for 30 min
revealing the presence of strontium silicate (SrSiO3) (PDF# 34-0099),
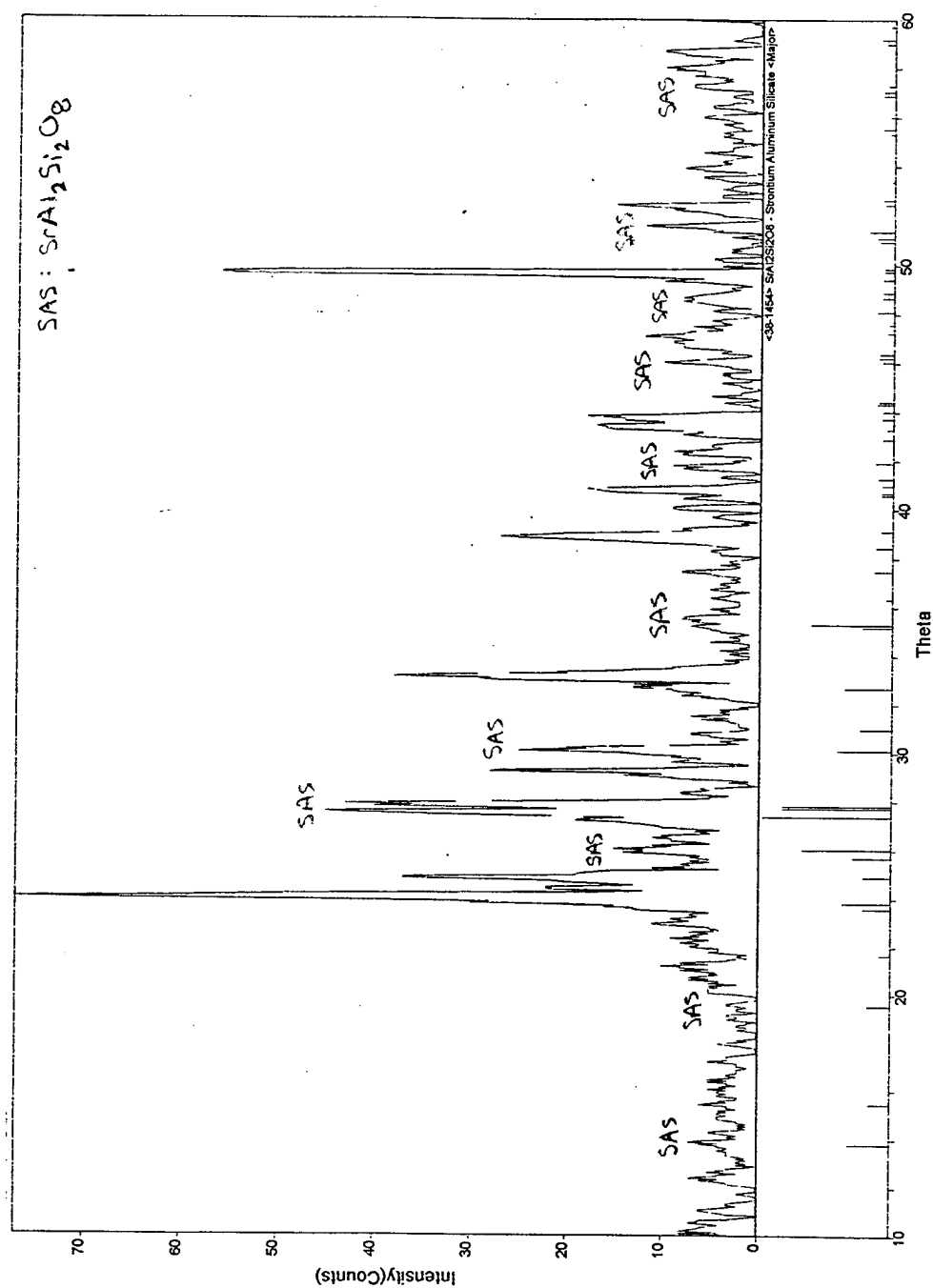errant peak at 2-Theta = 50 ° is possibly attributed to quartz substrate
(sample holder).

Fig. 13 XRD analysis of SAS-5 heat treated at 1000 °C for 5 hours, revealing the presence of crystalline strontium aluminum silicate ($SrAl_2Si_2O_8$) [celsian] and several other phases (PDF# 38-1454)

4.5.1 Temperature Regimes for Wetting.

Distinctive upper and lower temperature limits for wetting behavior were observed for each glass composition. For SAS-5 cubes on the Si_3N_4 substrates, wetting began at approximately 1300 °C and dissociation of $SiO_{2(l)}$ into $SiO_{(g)}$ (i.e. gas bubbles observed at the top of the molten glass inferred to be $SiO_{(g)}$) was observed at around 1480 °C. Matrix wetting experiments were carried out at temperatures of 1350 °C, 1400 °C, and 1450 °C for durations of 7.5, 15, and 30 minutes. For SAS-10 cubes on the Si_3N_4 substrates, wetting began at 1325 °C and dissociation of $SiO_{2(l)}$ into $SiO_{(g)}$ and $O_{(g)}$ was observed at around 1510 °C. Matrix wetting experiments were carried out at temperatures of 1400 °C, 1450 °C, and 1500 °C for durations of 15 and 30 minutes.

4.5.2 Contact Angle Measurements.

Contact angle measurements were taken at a constant temperature of 1325 °C for SAS-5 and SAS-10 glass cubes on the Si_3N_4 substrates. The same temperature was selected to allow for comparison between samples. Measurements were taken at one minute intervals. Results for each glass composition are presented in figure 14.
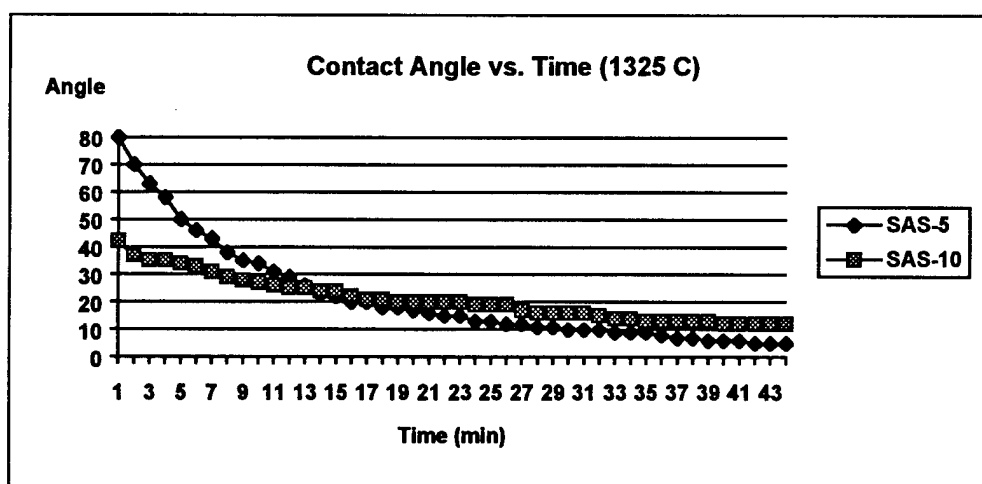
Fig. 14 Contact Angle Measurements

4.6 Electron Microprobe Analysis.

Microprobe analysis of the molten glass/substrate interface revealed a prominent diffusion zone for each wetting experiment. Microprobe analysis detected only cation concentrations and the analysis software calculated these concentrations as oxides, even though the Si was present as both an oxide (SiO_2) and as a nitride (Si_3N_4). Sr^{2+} ions penetrated into the Si_3N_4 substrate and Y^{3+} ions diffused into the molten glass. Diffusion of Y^{3+} ions also reveals a 30 - 40 μm wide depletion zone and then a small spike in concentration. Microprobe results are presented in figures 15-29; in each plot, the starting position for the distance scale was arbitrary.

Electron Microprobe Analysis

SAS-5 Composition on Si $_3$N$_4$ Substrate
1350°C 7.5 Min.
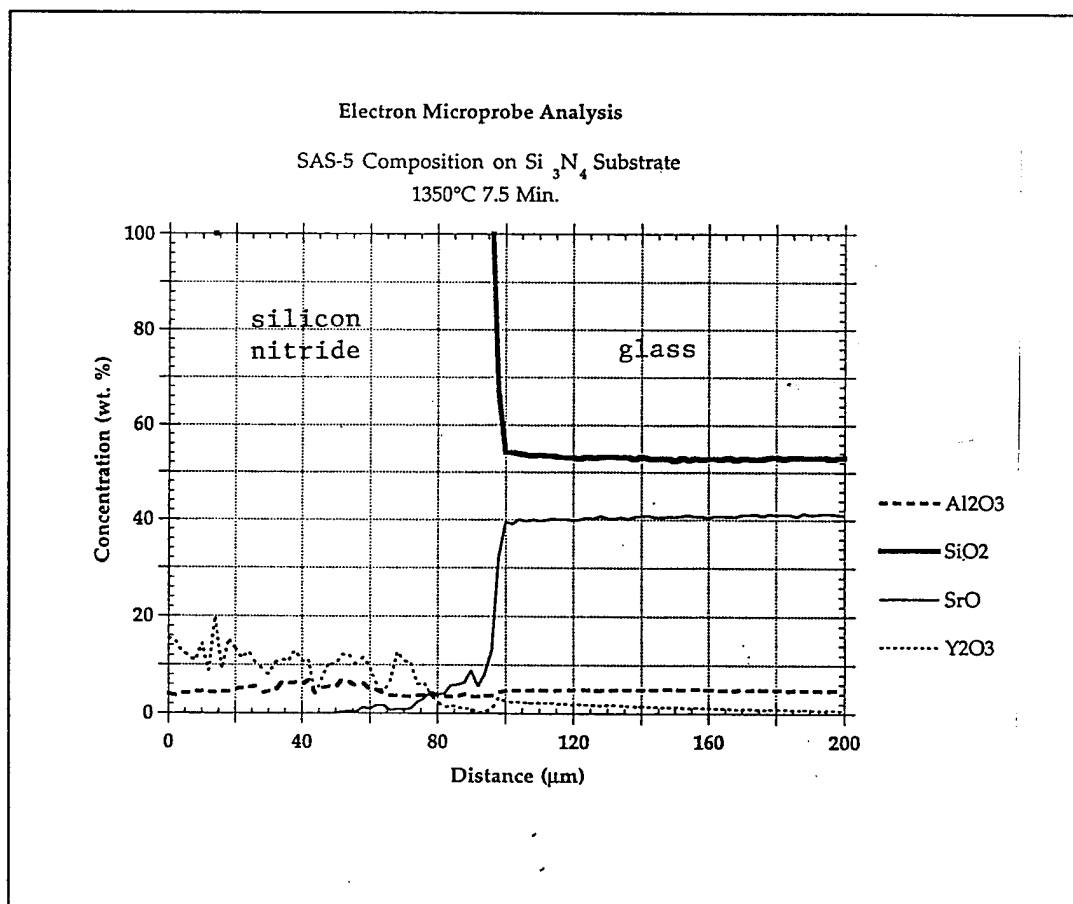
Fig. 15 Electron Microprobe for SAS-5 Wetting Si_3N_4: 1350 °C / 7.5 min
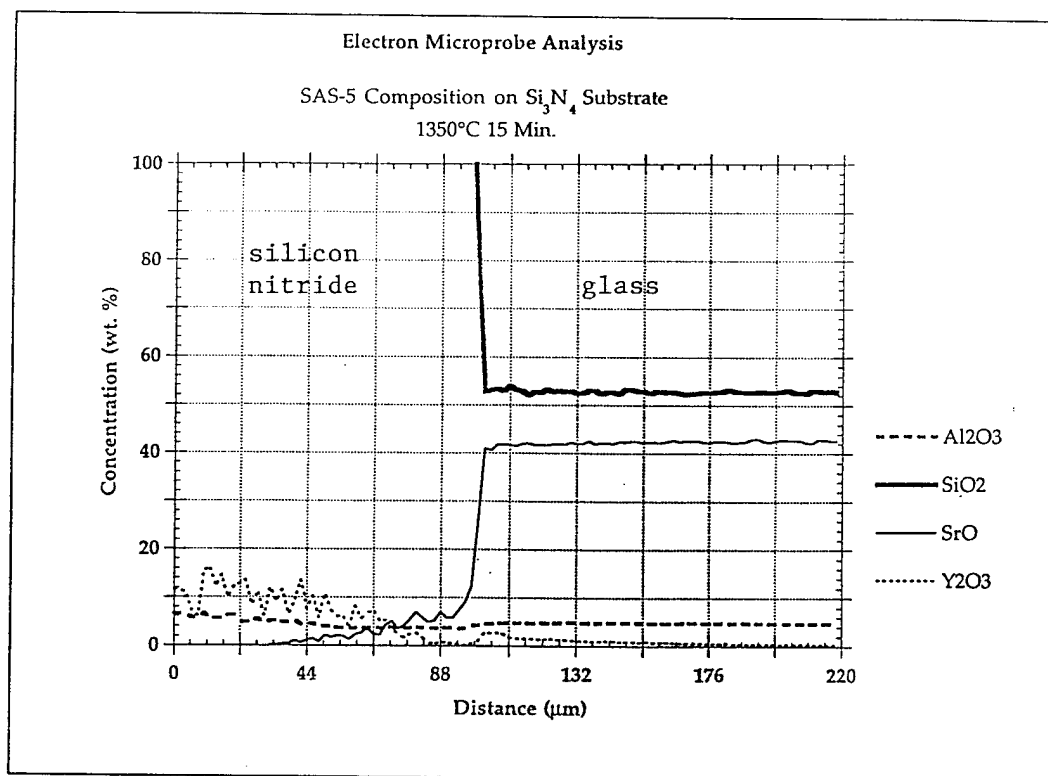
Fig. 16 Electron Microprobe for SAS-5 Wetting Si₃N₄: 1350 °C / 15 min
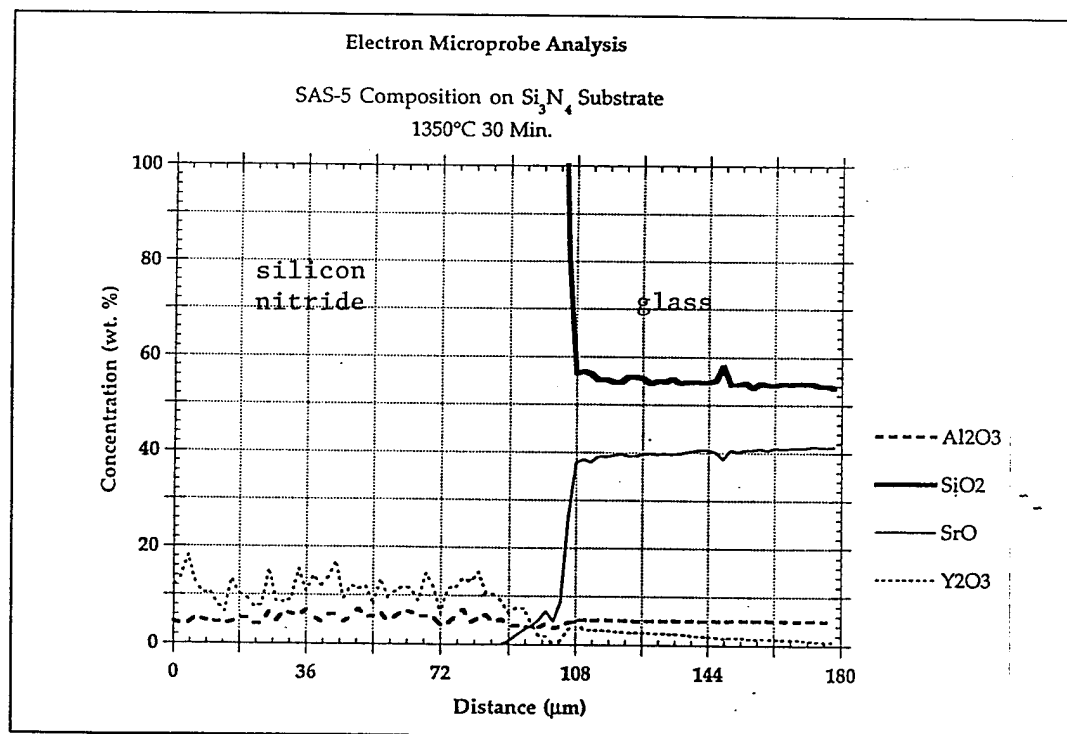
Fig. 17 Electron Microprobe for SAS-5 Wetting Si₃N₄: 1350 °C / 30 min
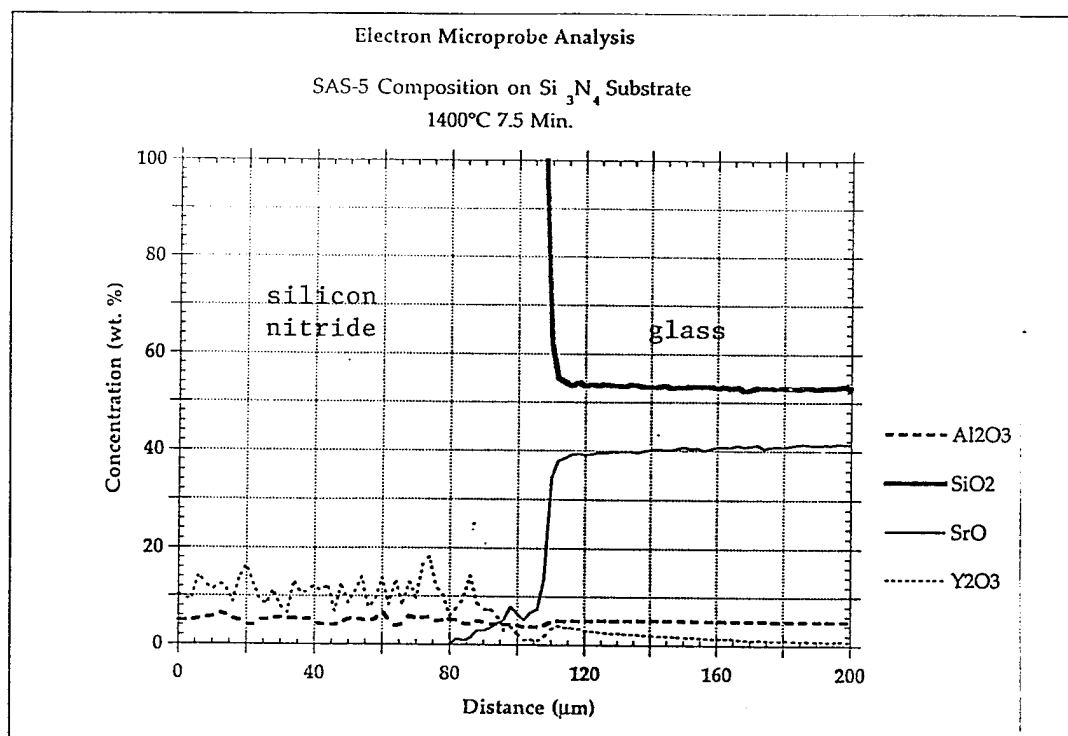
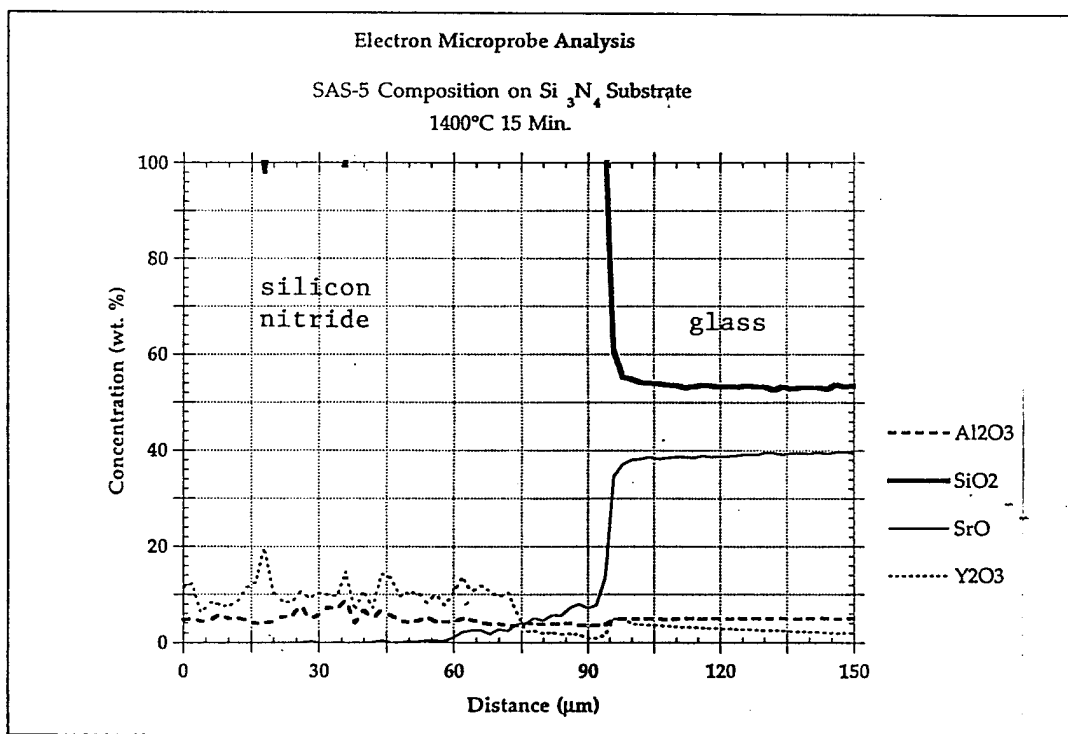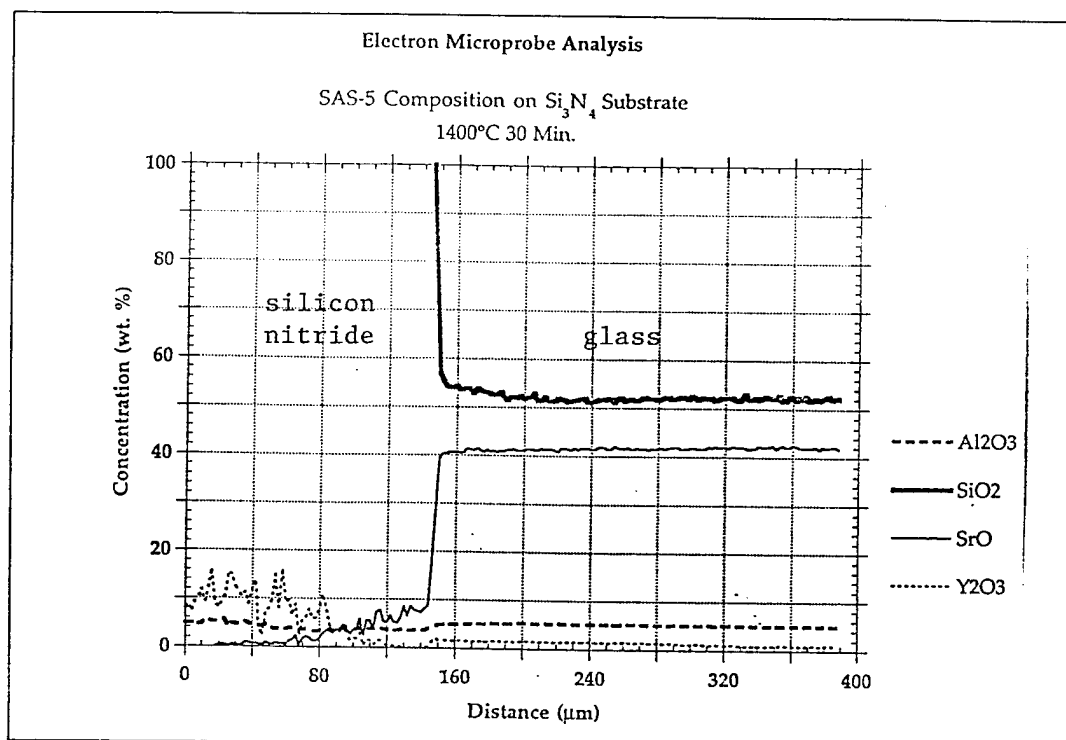**Fig. 18 Electron Microprobe for SAS-5 Wetting Si₃N₄: 1400 °C / 7.5 min**

Fig. 19 Electron Microprobe for SAS-5 Wetting Si₃N₄: 1400 °C / 15 min

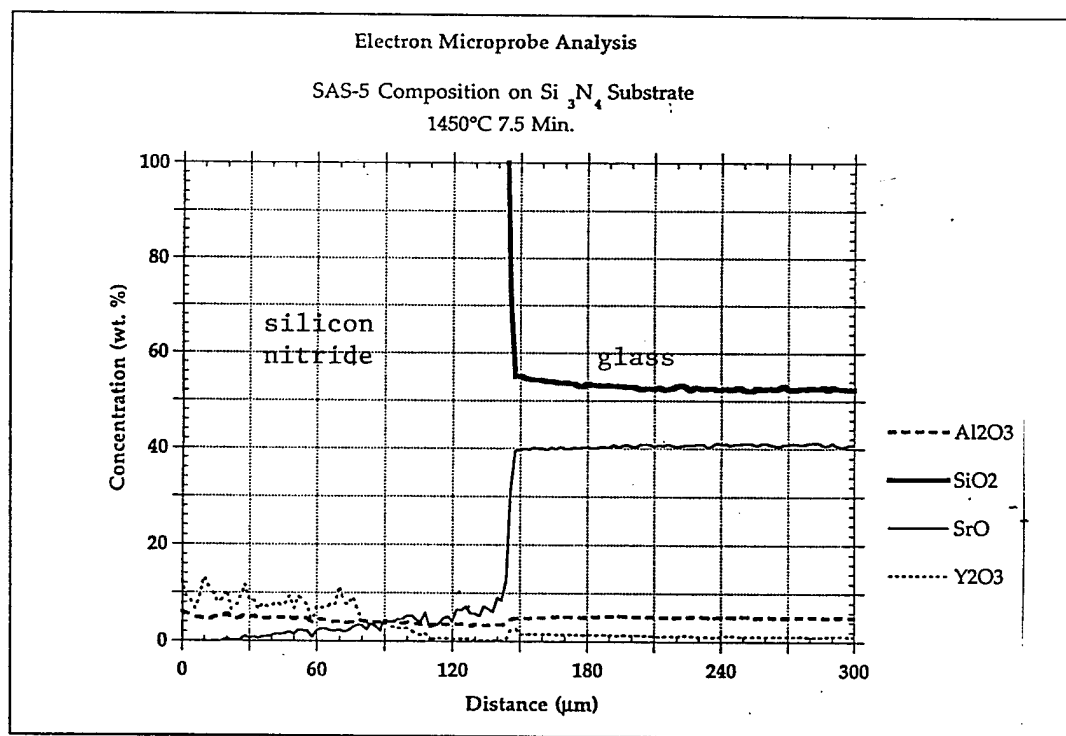Fig. 20 Electron Microprobe for SAS-5 Wetting Si_3N_4: 1400 °C / 30 min

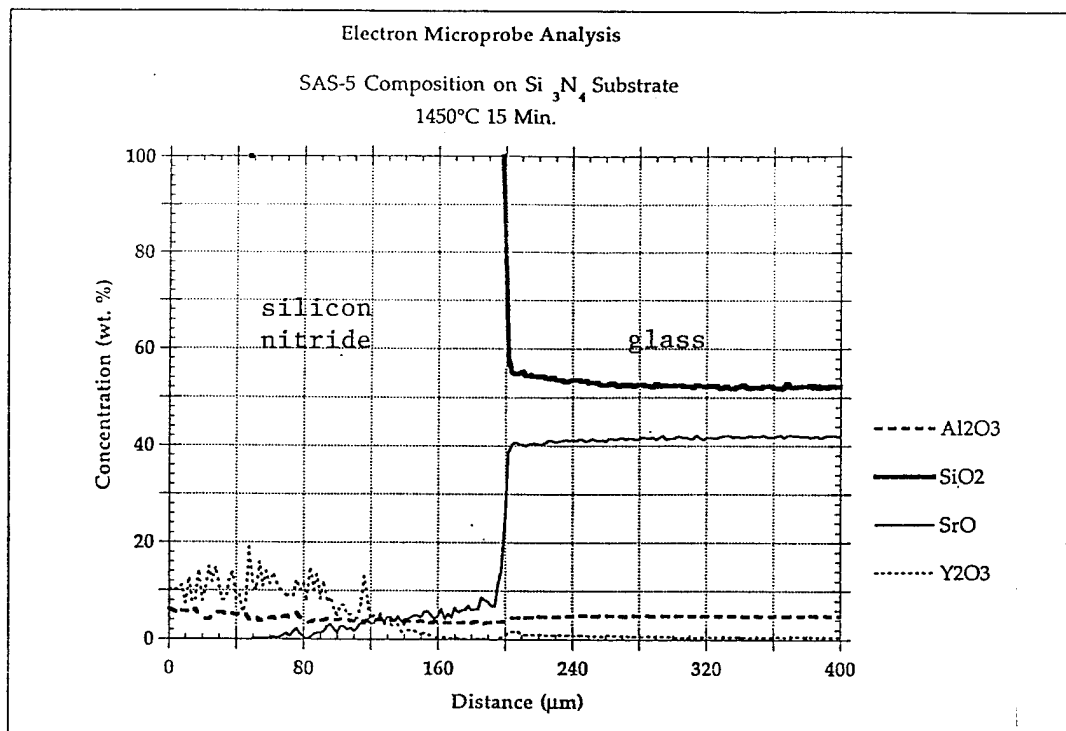Fig. 21 Electron Microprobe for SAS-5 Wetting Si_3N_4: 1450 °C / 7.5 min

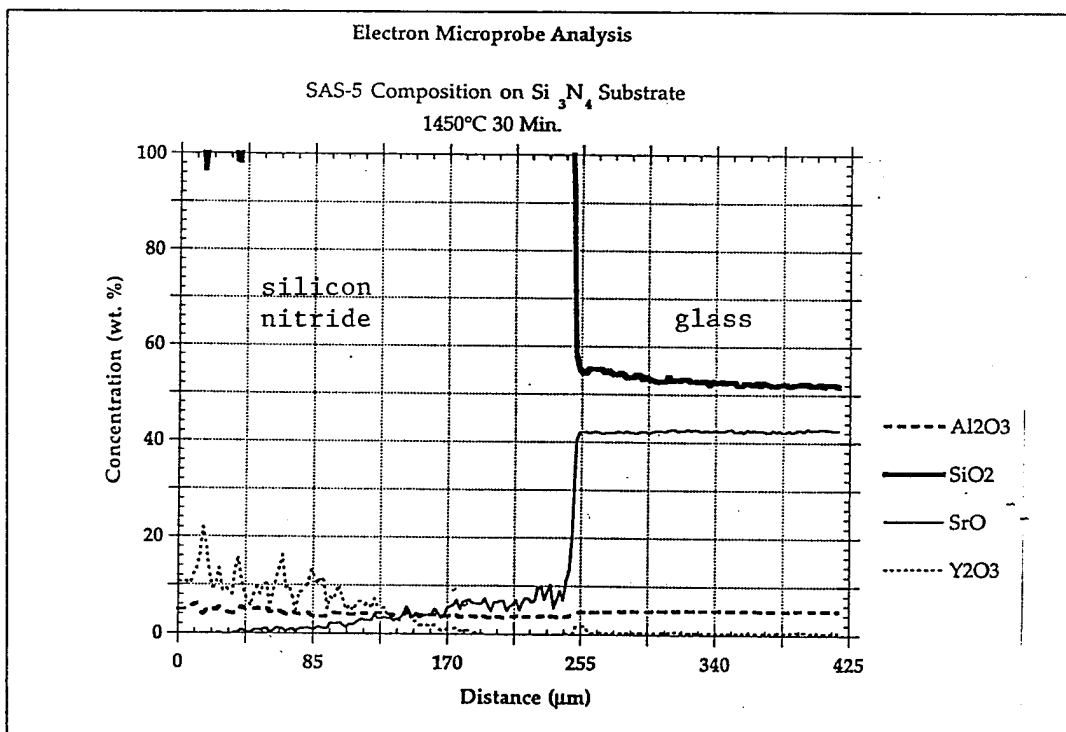Fig. 22 Electron Microprobe for SAS-5 Wetting Si₃N₄: 1450 °C / 15 min

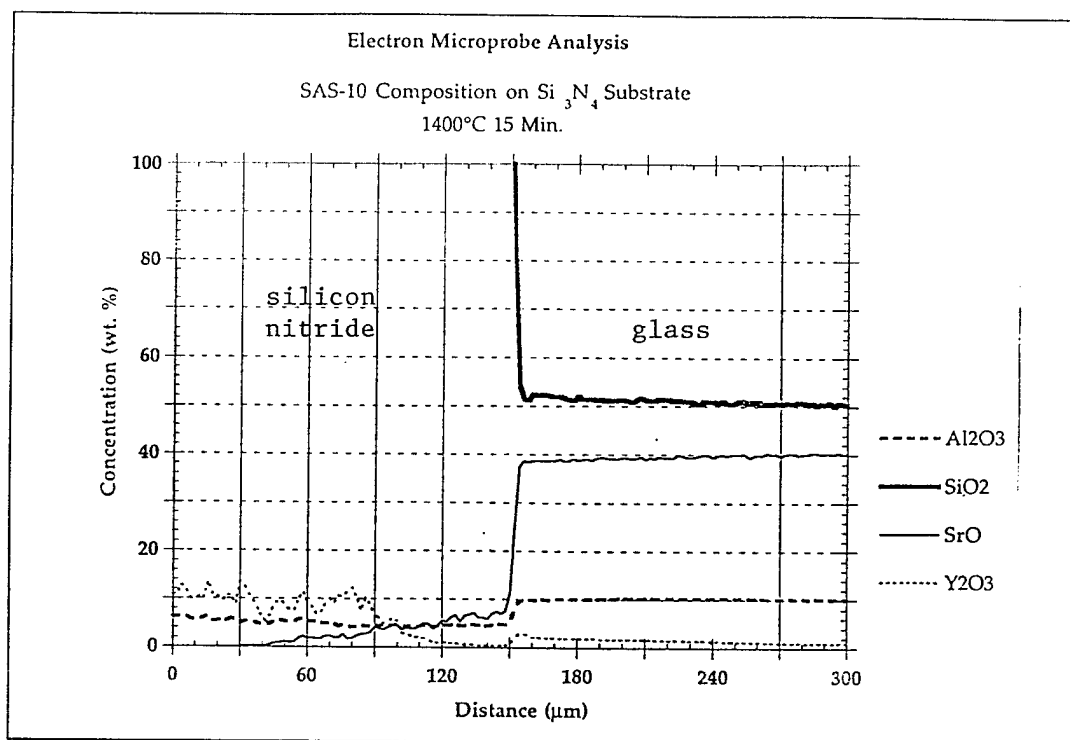Fig. 23 Electron Microprobe for SAS-5 Wetting Si₃N₄: 1450 °C / 30 min

Fig. 24 Electron Microprobe for SAS-10 Wetting Si₃N₄: 1400 °C / 15 min

Fig. 25 Electron Microprobe for SAS-10 Wetting Si₃N₄: 1400 °C / 30 min

Fig. 26 Electron Microprobe for SAS-10 Wetting Si₃N₄: 1450 °C / 15 min
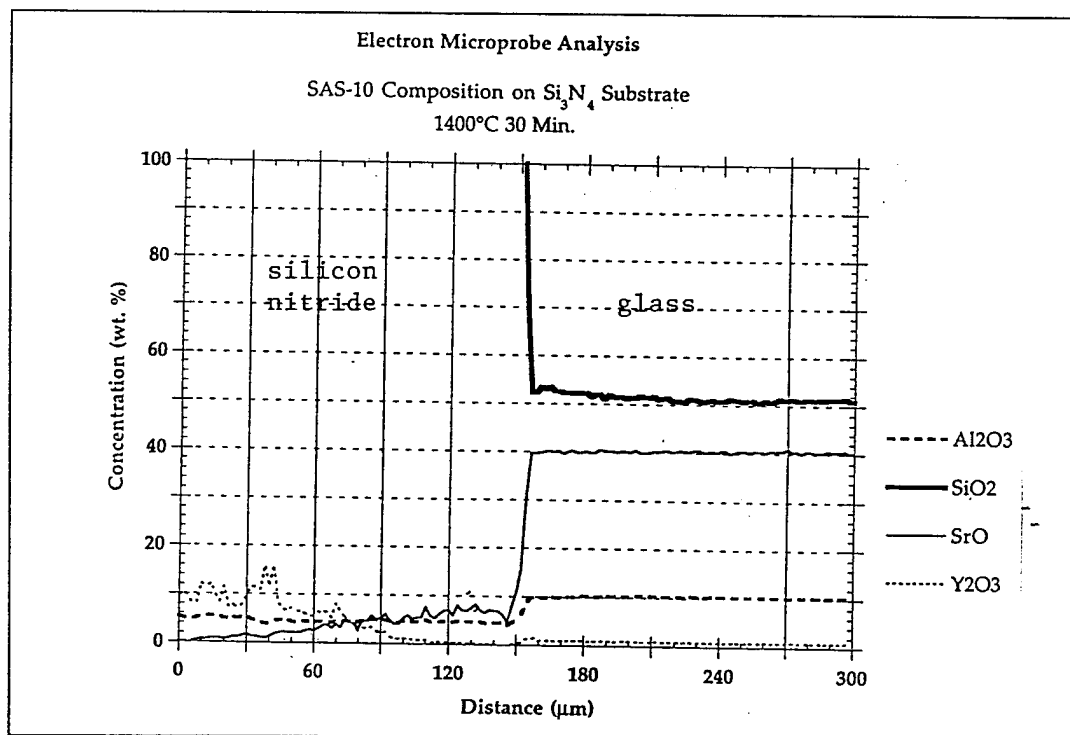

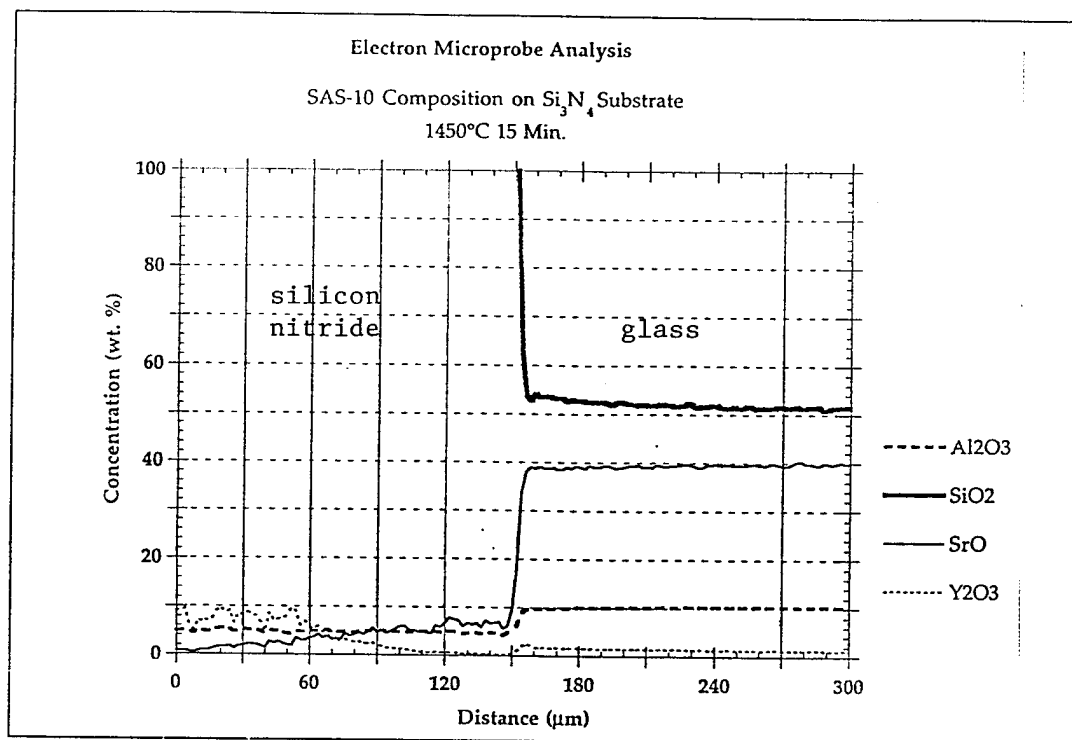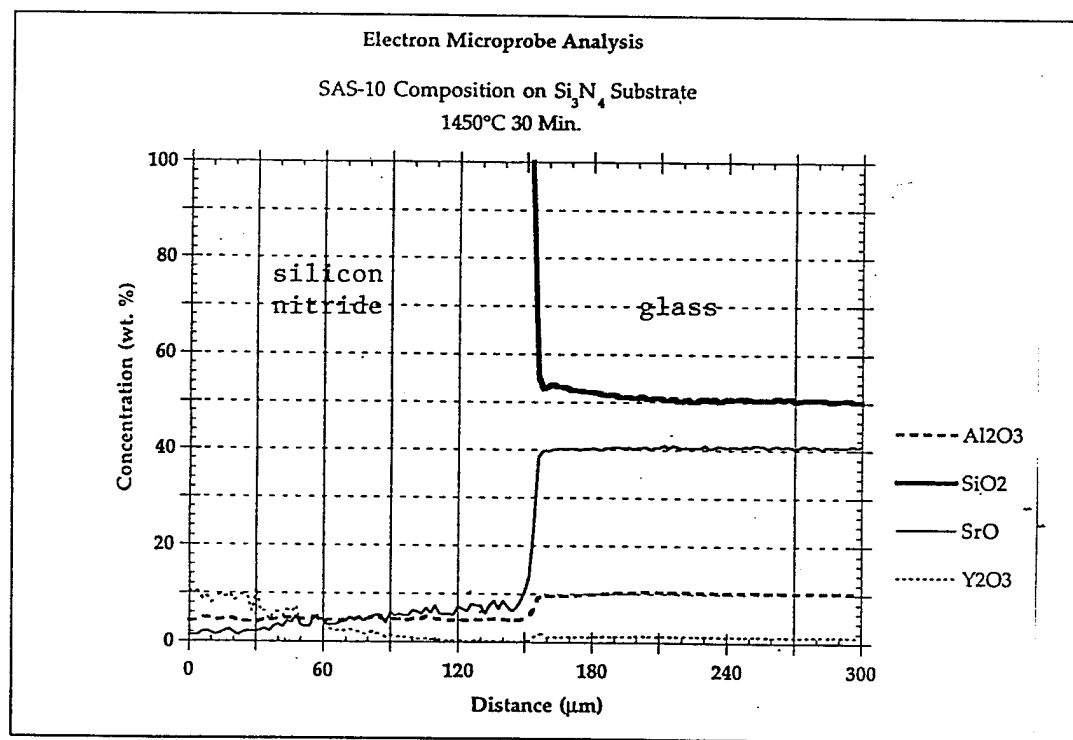**Fig. 27 Electron Microprobe for SAS-10 Wetting Si₃N₄: 1450 °C / 30 min**
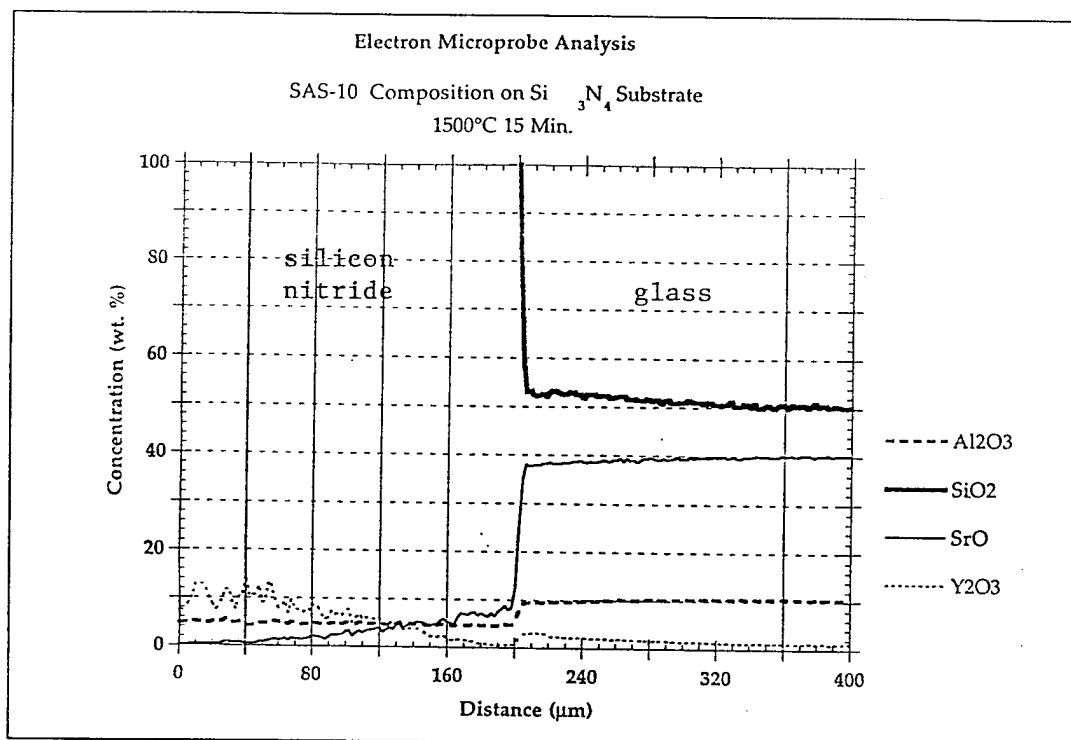
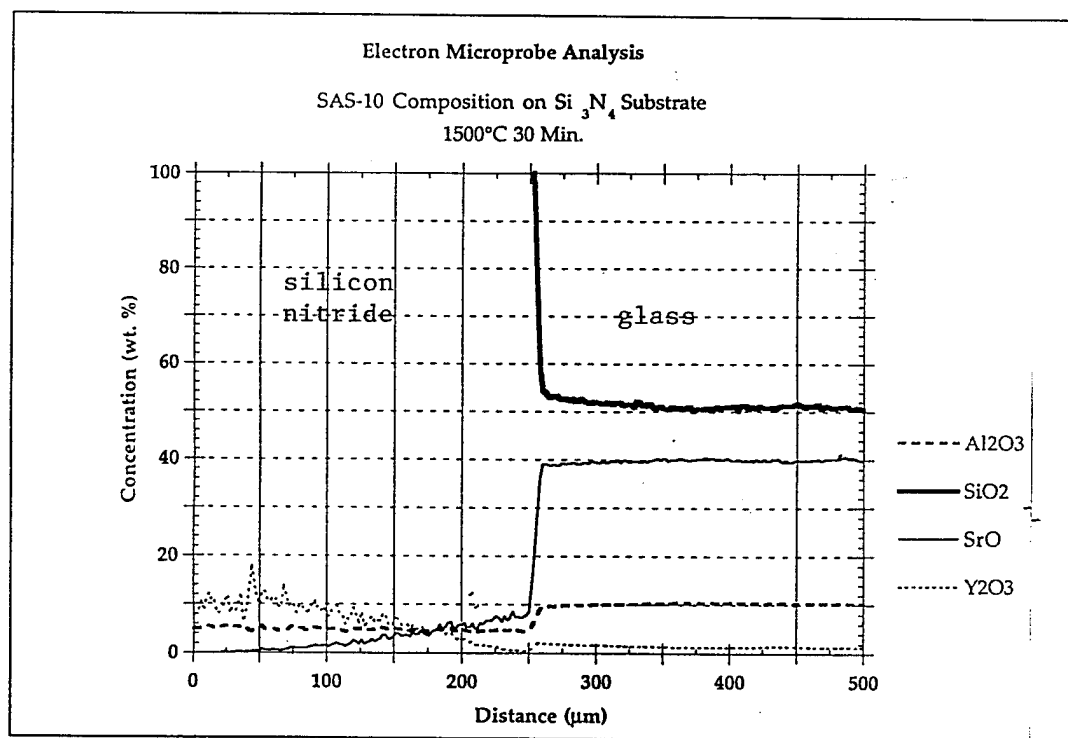Fig. 28 Electron Microprobe for SAS-10 Wetting Si_3N_4: 1500 °C / 15 min

Fig. 29 Electron Microprobe for SAS-10 Wetting Si_3N_4: 1500 °C / 30 min

4.7 XRD Analysis of Reaction Zone.

XRD analysis of the reaction zone at the interface of the wetted Si_3N_4 surface and the molten glass compositions revealed different crystalline compounds. SAS-5 glass wetting experiments, heated at 1325 °C for 78 minutes, revealed via XRD the presence of β-Si_3N_4 (PDF# 33-1160) and strontium aluminum oxide ($Sr_4Al_2O_7$, PDF# 28-1204) (see figure 30). XRD analysis of this reaction zone in SAS-5 wetting experiments heated at 1425 °C for 30 min and in SAS-10 wetting experiments heated at 1550 °C for 7.5 min showed mostly glass and a small amount of β-Si_3N_4 as the only crystalline phase (figures 31 and 32).
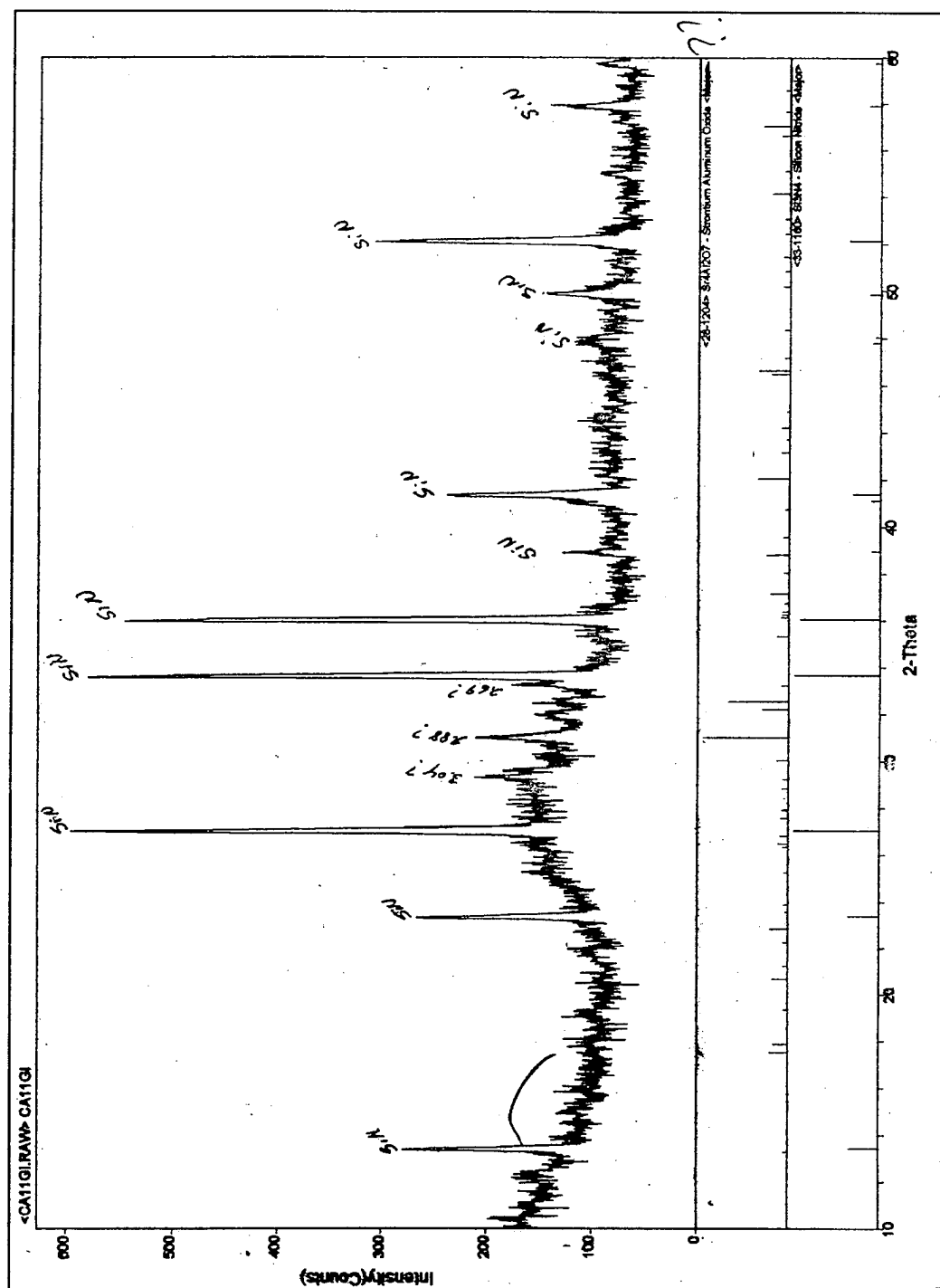
Fig. 30   XRD analysis of the reaction zone of SAS-10 glass wetting Si3N4 at 1325°C for 78 min revealing the presence of Si3N4 (PDF# 38-1160) and possibly strontium aluminum oxide (Sr4Al2O7) (PDF# 28-1204).

Fig. 31 XRD analysis of the reaction zone of SAS-5 glass wetting Si_3N_4 at 1425 °C for 30 min showing mostly glass and a small amount of Si_3N_4 (PDF# 33-1160) as the only crystalline phase.

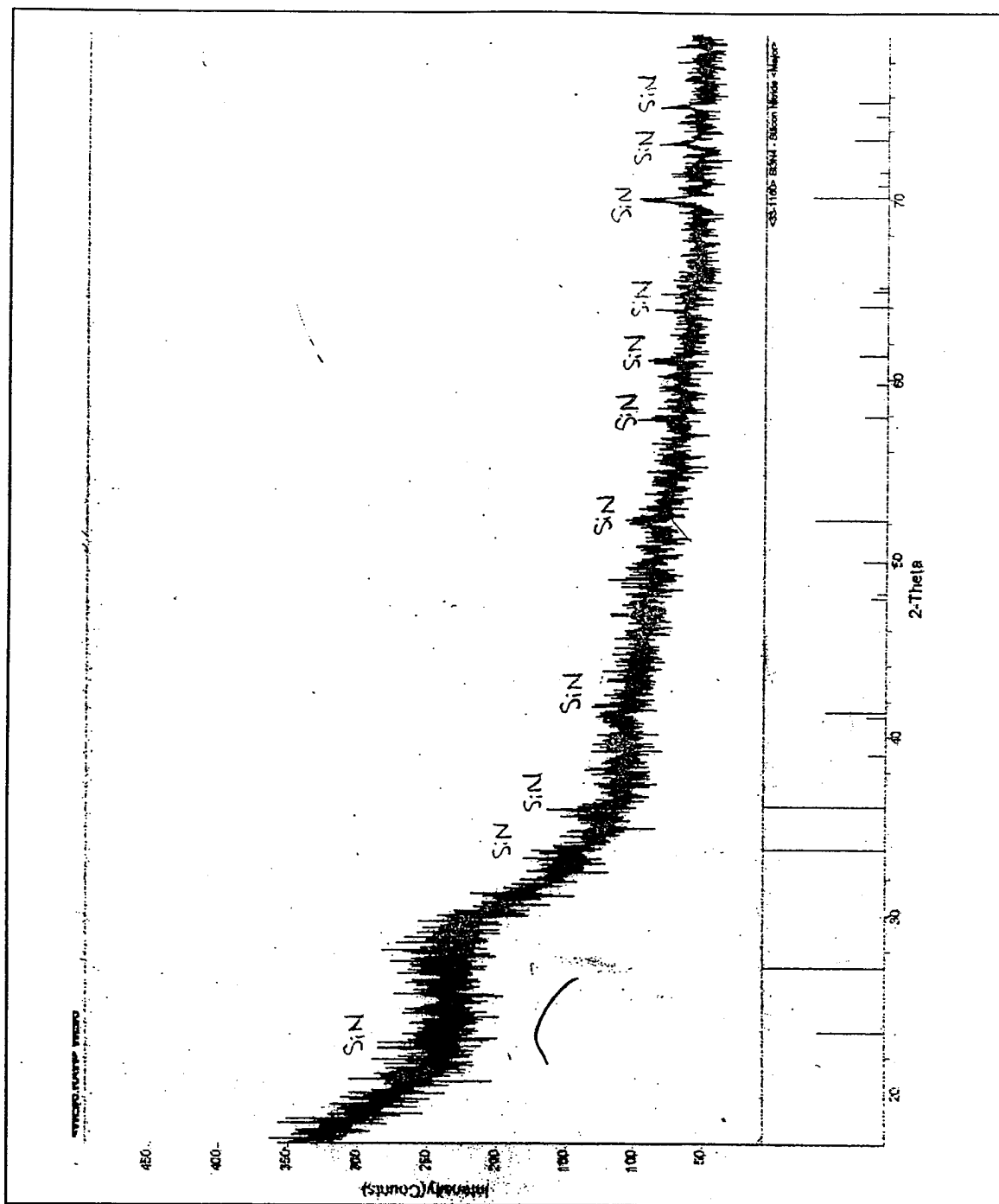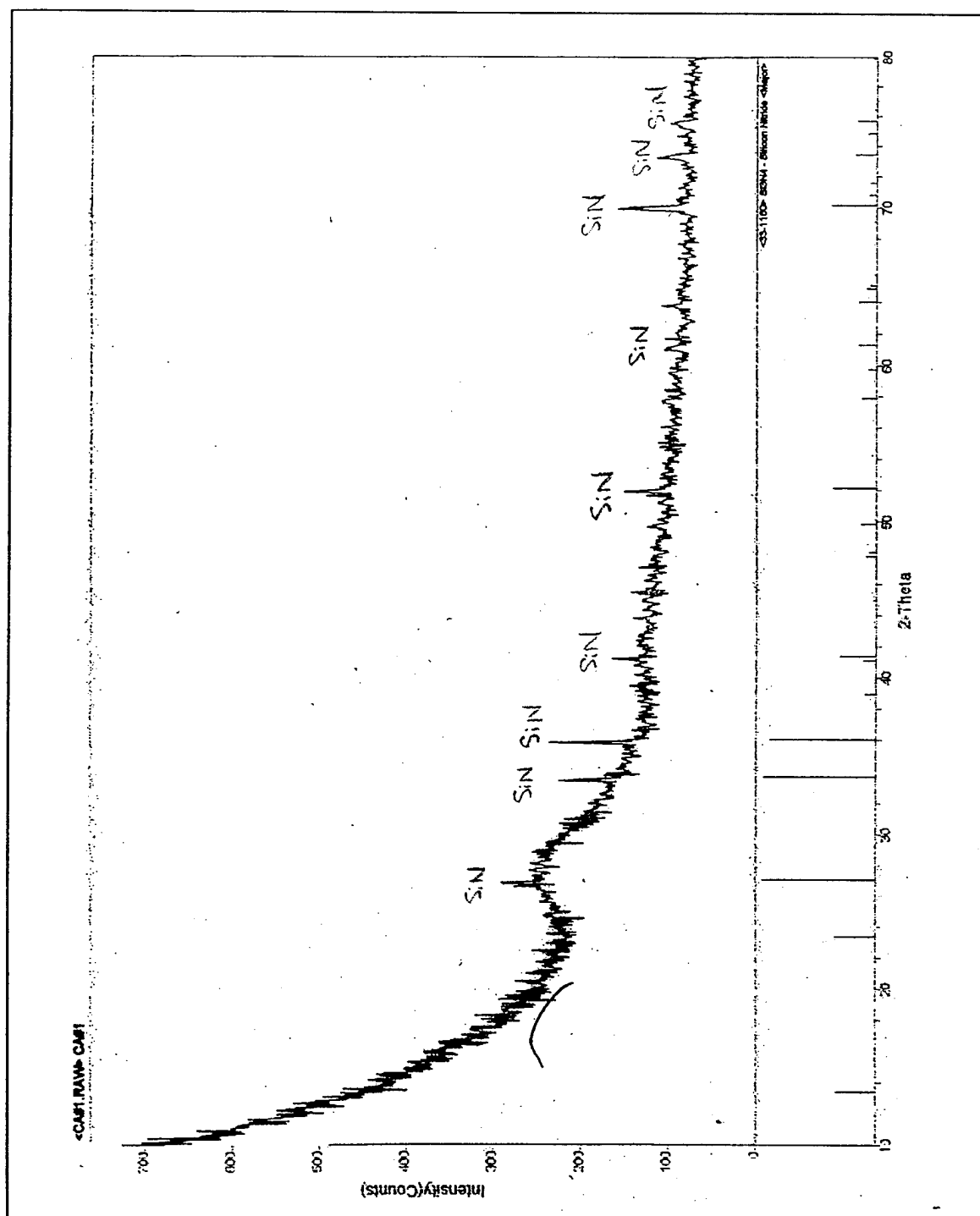Fig. 32 XRD analysis of the reaction zone of SAS-10 wetting Si3N4 at 1550 °C for 7.5 min showing mostly glass and a small amount of Si3N4 (PDF# 33-1160) as the only crystalline phase.

4.8   Electron Imagery of Wetting Results

BSE images of wetted Si3N4 substrates reveal prominent diffusion zones. Additionally, elemental distribution micrographs tracing Y, Al, and Sr concentrations across the interface show the movement of ions between the glass and the Si3N4. Representative BSE images of SAS-5 and SAS-10 wetted Si3N4 are presented in figures 33 and 34, respectively. These figures also reveal dissolution of Si3N4 grains at the interface.
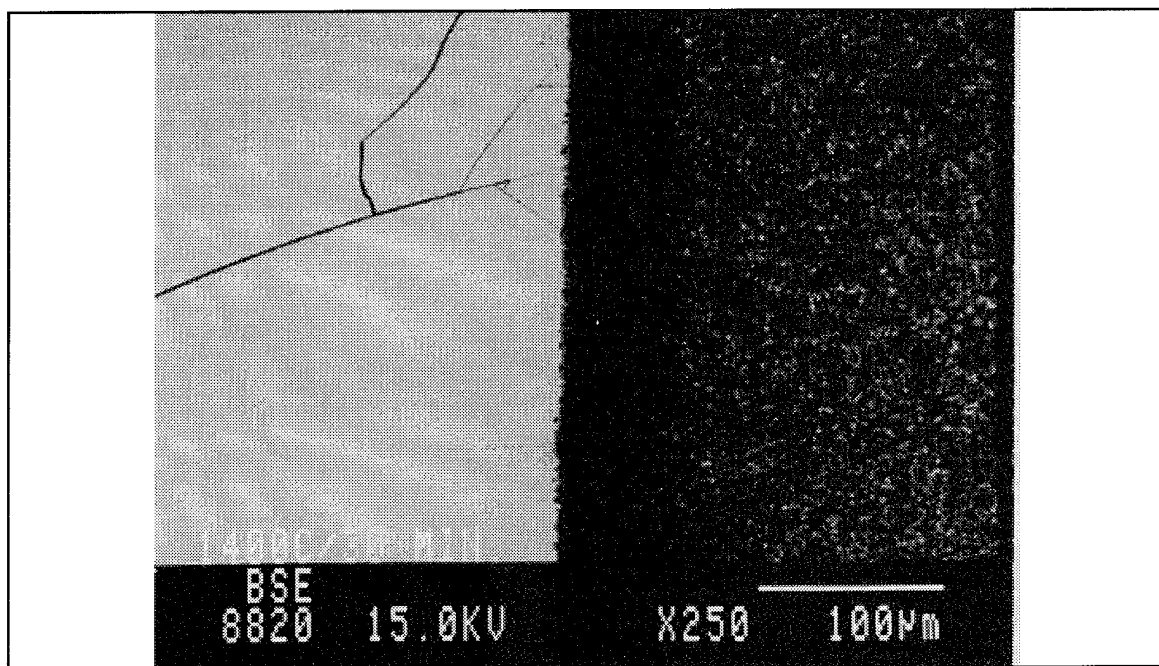
Fig. 33   BSE Image of SAS-5 Glass Wetting Si3N4 with Heat Treatment of 1400 °C for 30 min (magnification: 250x)   [glass is left of substrate]
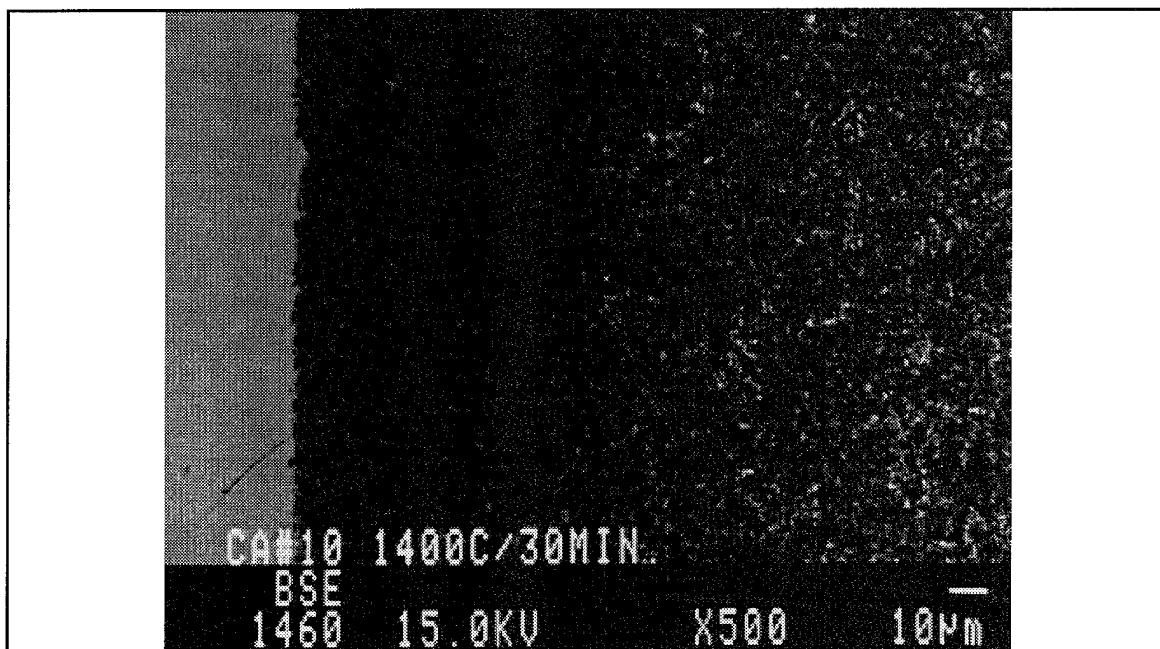
Fig. 34 BSE Image of SAS-10 Glass Wetting Si3N4 with Heat Treatment of 1400 °C for 30 min (magnification: 500x) [glass is left of substrate]

A representative Y distribution micrograph for SAS-5 wetting Si3N4 is presented in figure 35, revealing strong concentrations of Y in the substrate and Y diffusion into the glass (most likely as Y^{3+} ions). It also reveals a 30-40 µm wide depletion zone for Y concentration at the interface. This depletion zone is also evident in electron microprobe data presented in section 4.6.

Fig. 35   10% Y Distribution Micrograph for SAS-5 Glass Wetting Si3N4 at 1400 °C for 30 min (magnification: 500x) [glass is left of substrate]

A representative Sr distribution micrograph for SAS-5 wetting is presented in figure 36 and clearly shows the diffusion of Sr^{2+} ions from the glass into the Si3N4 during wetting.

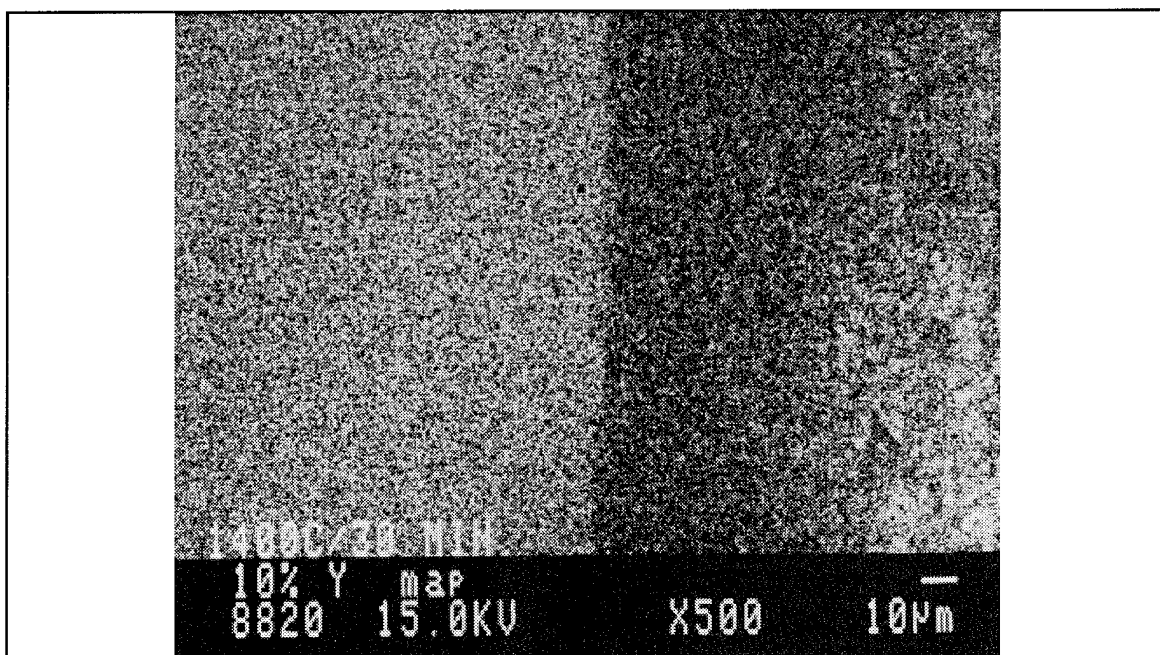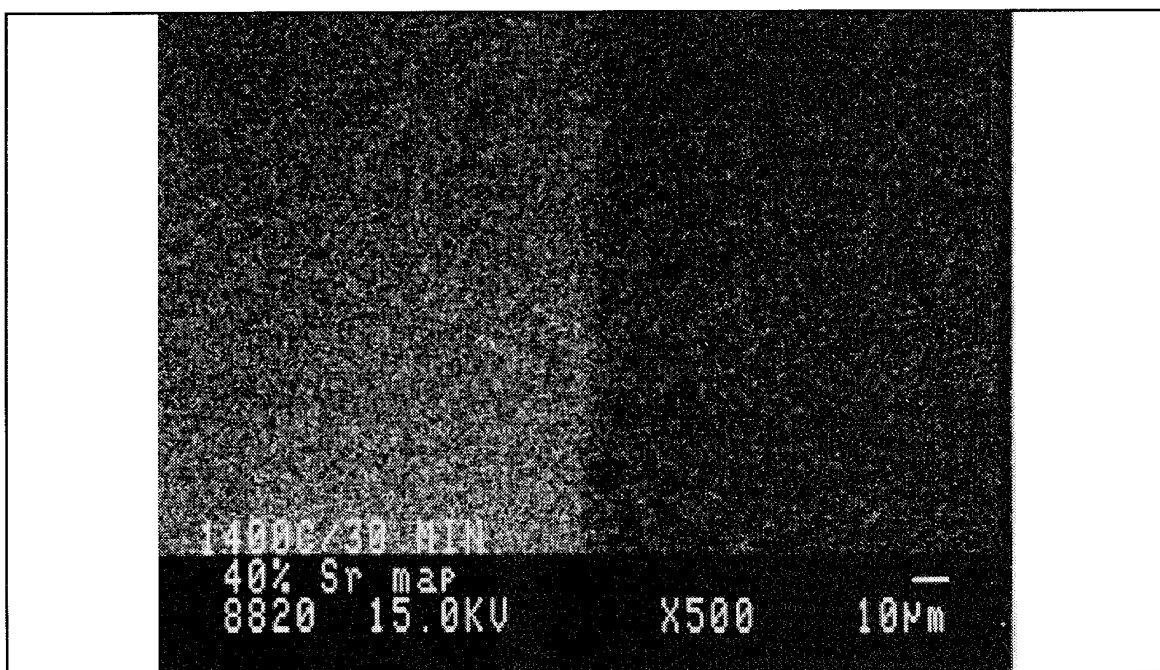**Fig. 36   40% Sr Distribution Micrograph for SAS-5 Glass Wetting Si3N4 at 1400 °C for 30 min (magnification: 500x) [glass is left of substrate]**

A representative Al distribution micrograph for SAS-5 wetting is presented in figure 37. This 10% distribution map reveals Al in both the glass composition and the Si3N4 substrate. It also serves to highlight the similar levels of Al concentration; it is almost impossible to distinguish the interface between the glass and the substrate.
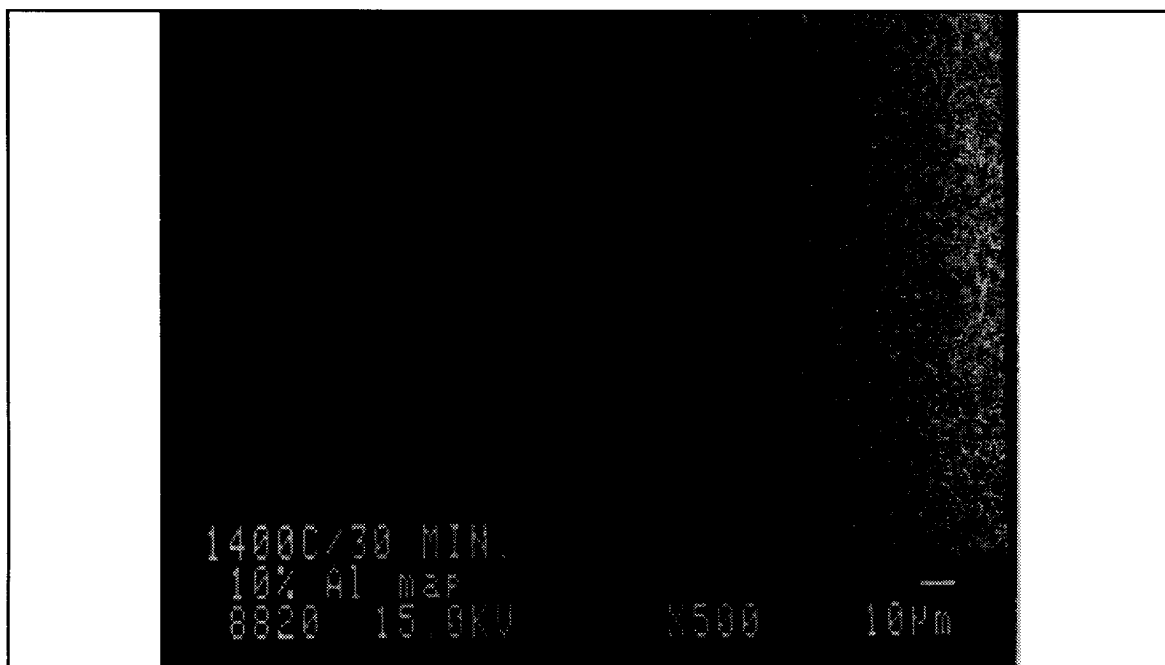
Fig. 37 10% Al Distribution Micrograph for SAS-5 Glass Wetting Si3N4
at
1400 °C for 30 min (magnification: 500x) [glass is left of substrate]

4.9 Four-Point Bending Results

Four-point bending tests conducted on size B bend bars (IAW MIL-STD 1492A) (*30*) joined using SAS-5 and SAS-10 interlayers revealed promising results. Bending tests were conducted on bars sectioned from the end and middle sections of the joined plates. Bars were numbered one through nine, with one and nine being the end pieces. The maximum strength achieved using the SAS-5 glass interlayer was 469.6 MPa, which corresponds to an absolute peak minimum load of 563.7 N. The maximum strength achieved using the SAS-10 interlayer was 378.5 MPa, which corresponds to an absolute peak minimum load of 454.4 N. Strength measurements were taken at room temperatures of 79.2 and 76.6 °F for SAS-5 and SAS-10 joining, respectively. The results for all of the bend bars tested are presented in tables 4 and 5. The highest strength test bar for the SAS-5 joined plates was sectioned from the middle of the sample, whereas the strongest test bar

for the SAS-10 joined plates was sectioned from the end of the sample.

**Table 4   Four-Point Bending Results for Si3N4 Plates
Joined Using a SAS-5 Interlayer**

Bar Number	Position with respect to center of joined plates	Absolute Peak Minimum Load (N)	Four-Point Strength (MPa)
1	End	96.38	80.3
2		200.36	166.9
4	Center	563.7	469.6
6		112.49	93.7
8	End	94.93	79.07

Joints formed using SAS-5 glass appeared to break primarily in the joint region. Bar 4, with the highest strength, however, fractured in the joint region and the adjoining Si3N4. Glass coverage of the Si3N4 pieces appears to have been more complete in bars sectioned from the middle of the joined plates (bars 2, 4, and 6).

**Table 5   Four-Point Bending Results for Si3N4 Plates
Joined Using a SAS-10 Interlayer**

Bar Number	Position with respect to center of joined plates	Absolute Peak Minimum Load (N)	Four-Point Strength (MPa)
1	End	454.35	378.5
2		334.75	278.9
3		241.58	201.2
4	Center	249.03	207.4
6		168.51	140.4
8	End	173.51	144.5

Fractures observed in these test bars joined using the SAS-10 interlayer appear to have occurred mainly in the joint region, with possibly slight fractures in the adjoining Si_3N_4 (especially in bar 1). As in the four-point bending results for SAS-5 joined plates, glass coverage in the SAS-10 joined bars appears to have been uneven. Coverage was more complete for test bars one and two, at the end of the joined plates, compared to the other test bars.

5 DISCUSSION OF RESULTS

5.0 General

The objectives of this research were to evaluate the thermal stability of the SiO_2-SrO-Al_2O_3 glass system, determine the bonding mechanisms for reaction and inter-penetration of the glass and Si_3N_4, and demonstrate the successful joining of Si_3N_4 using this glass without applying high pressure. A homogeneous glass mixture was used instead of an unreacted powder batch to avoid the need for very high joining temperatures to form a melt. This also avoided the occurrence of heterogeneous reactions which do not necessarily involve all of the components and which would hinder bonding.

5.1 SiO_2-SrO-Al_2O_3 Glass Behavior and Stability

SAS-5 and SAS-10 compositions were based on the addition of Al_2O_3 to the SiO_2-SrO eutectic composition with the lowest liquidus temperature. From the SiO_2-SrO equilibrium phase diagram (figure 38), this composition is 54 wt% SiO_2 - 46 wt% SrO. Only 5 and 10 wt % additions of Al_2O_3 were made to this base composition in order to keep glass melting temperatures low and attain higher viscosities at joining temperatures.
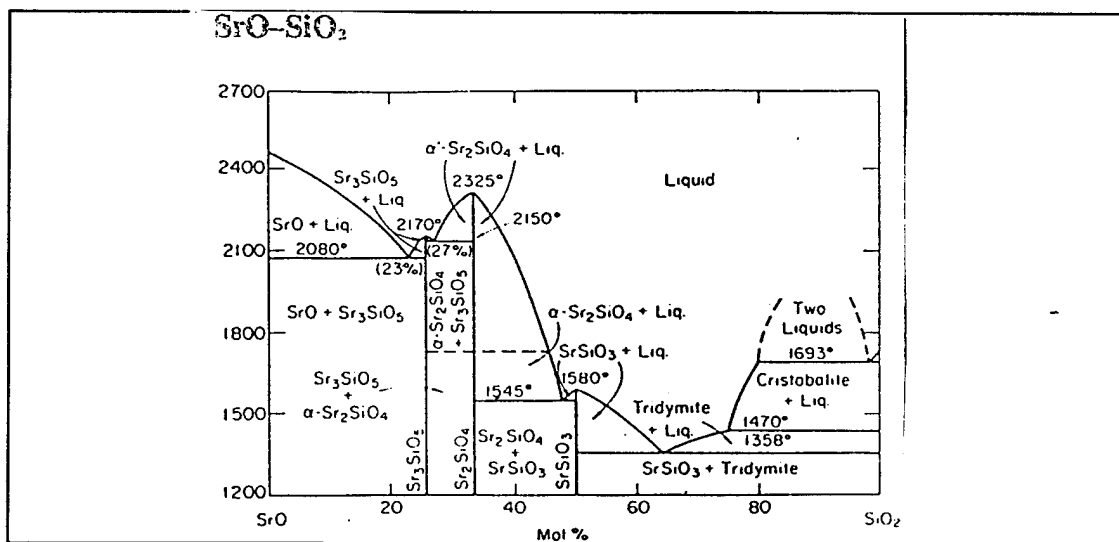

Fig. 38 SiO_2-SrO Equilibrium Phase Diagram (24)

5.1.1 Thermal Stability of the SiO₂-SrO-Al₂O₃ Glass System

The high temperature stability characteristics of these glasses are evident from crystallization behavior and CTE measurements. In terms of CTE, dilatometer measurements for SAS-5 and SAS-10 compositions reveal values of 8.54×10^{-6} /°C and 8.46×10^{-6} /°C, respectively, a difference of less than one percent (well within the error tolerance for measurement). As a result, differences in thermal stability must be examined in terms of crystallization behavior. Crystallization expectations are based on the ternary SiO₂-SrO-Al₂O₃ equilibrium phase diagram (figure 39).
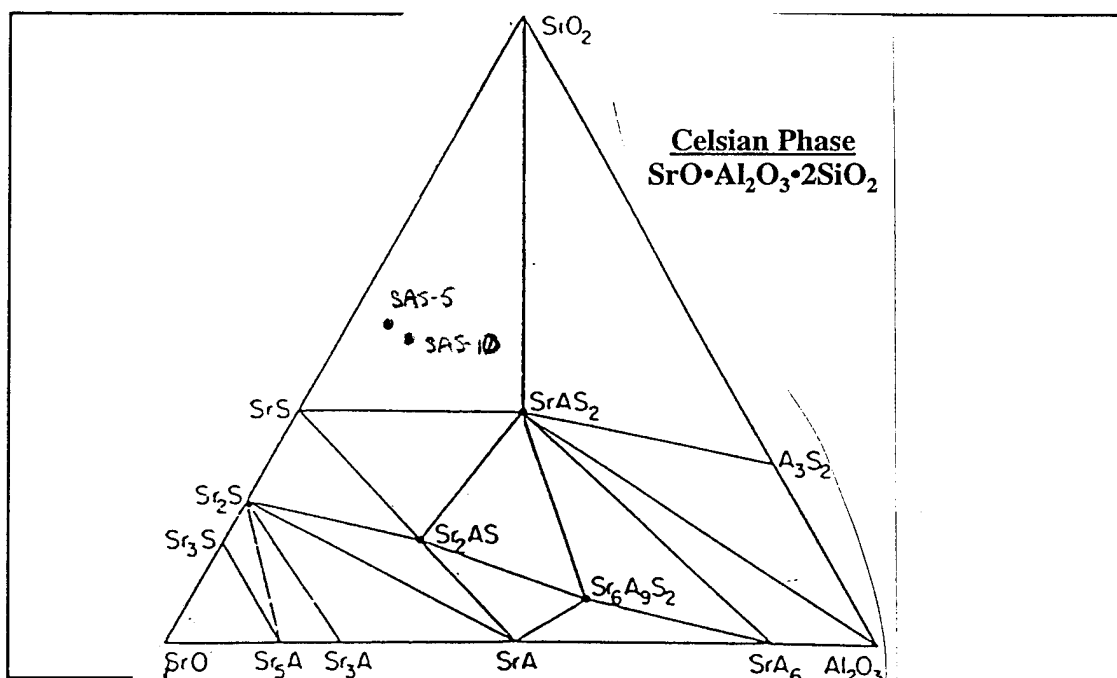
Fig. 39 SiO₂-SrO-Al₂O₃ Ternary Equilibrium Phase Diagram in wt% [1350 °C] (*24*)

Celsian crystallization is represented as the SrAS₂ (SrO-Al₂O₃-2(SiO₂)) composition at the center of the diagram. Based on this phase diagram, it is expected that SAS-5 and SAS-10 glasses would crystallize into a three phase equilibrium consisting of SrS (SrO-SiO₂) and SiO₂ phases along with a celsian phase. XRD analysis of SAS-5 crystallization heat treatment (figure 11) confirms this crystallization of SrS at 1200 °C.

Furthermore, XRD analysis of the bottom surface of furnace-cooed SAS-5 heat treated at 1000 °C for five hours shows evidence of celsian crystallization (figure 12). These results imply very slow celsian crystallization in the 5 wt% SAS-5 composition. SAS-10 samples, on the other hand, demonstrated a high resistance to crystallization at any temperature. Even a five hour heat treatment did not result in any crystallization. This result is indicative of the stability of the glass which is due to the increased Al_2O_3 content.

5.1.2 High Temperature Stability

The crystallization results discussed above present some important aspects of this glass system's high temperature stability. Crystallization in the joint region is desired to precipitate out the celsian phase so as to achieve a match in the CTE of the joint and the Si_3N_4 substrate. The CTE of celsian is 2.29×10^{-6} /°C compared to 3.3×10^{-6} /°C for this commercial Si_3N_4. It is anticipated that a completely amorphous joint region would not provide sufficient strength at engine operating temperatures as high as 1370 °C. Possible crystallization of celsian in SAS-5 samples is promising in terms of being able to utilize celsian's low CTE in joining. The resistance to crystallization demonstrated by the higher Al_2O_3 content SAS-10 is expected due to the glass forming and strengthening characteristics offered by Al_2O_3. The addition of a nucleating agent, such as colloidal Pt, ZrO_2, or Li_2O, should result in a more rapid crystallization of celsian in both glass compositions. Overall, these results are promising in terms of future efforts to employ heat treatments to crystallize the joint region in joined Si_3N_4 pieces.

5.2 Wetting Behavior

Wetting behavior is best described in terms of Young's Equation (as discussed in *29*):

$$\gamma_{sv} - \gamma_{sl} = \gamma_{lv} \cos\theta$$

where γ_{sv}, γ_{sl}, and γ_{lv} represent the surface free energy (or tension) of the solid/vapor,

solid/liquid, and liquid/vapor, respectively; and θ is the contact angle (see figure 40). This

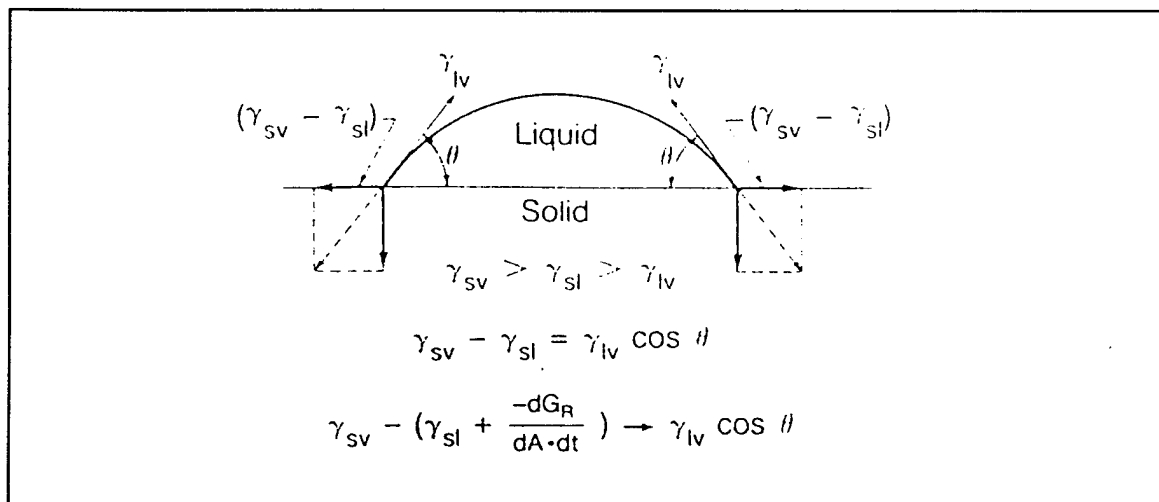equation represents a balance of forces at steady-state conditions at the periphery of

Fig. 40 Young's Equation and Wetting Behavior (from *Ref 29*)

the sessile drop. The driving force for extension of the liquid drop is the reduction of the

surface free energy of the solid by the liquid (γ_{sv} - γ_{sl}). The balancing resisting force is the

horizontal component of the liquid surface tension ($\gamma_{lv} \cos\theta$). In the presence of reaction

between the liquid drop and the substrate, this equation is modified to include the

contribution of the free energy of reaction, which contributes to the driving force for

wetting:

$$\gamma_{sv} - \left(\gamma_{sl} + \frac{\Delta G_R}{dA_s dt}\right) \geq \gamma_{lv} \cos\theta$$

where A_s is the surface area of the drop and ΔG_R represents the Gibbs free energy of

reaction. In this system, wetting of the Si_3N_4 is driven by a lowering of its interfacial

energy by the molten glass systems. Wetting is enhanced (and the contact angle reduces

further) by the dissolution reaction of Si_3N_4 grains at the interface. In terms of

comparison, contact angle measurements for SAS-5 and SAS-10 compositions (figure 14)

show SAS-10 begins with a faster rate of reduction in contact angle up to 1325 °C (40 °

vs. 80°). However, this initial difference is overcome by the more rapid reduction in contact angle exhibited by SAS-5 at constant temperature. Both glasses leveled off to equilibrium contact angles of less than 10°. SAS-5 glass reached an equilibrium contact angle of 5° at 44 min and SAS-10 reached an equilibrium angle of 8° at 65 min (although not depicted in figure 13). It is expected that each system would have eventually reached zero degree contact angles, but further reduction in the contact angles were impeded when the glass sessile drops reached the edge of the substrate (where surface tension at the edge provided more resistance to wetting). In contact angle measurements for both glasses, 1325 °C is at the low end of the temperature regime observed for wetting.

5.3 Chemical Bonding Mechanisms

The primary bonding mechanism involved in this joining method is the inter-diffusion of cations. Electron microprobe analysis of wetted Si_3N_4 substrates (figures 15 - 29) revealed significant diffusion of components between the glass and the substrate. Diffusion of Sr^{2+} from the glass into the substrate was significant and the penetration distance varied with joining temperature (figures 41 and 42). This diffusion pattern is also very evident in Sr elemental distribution micrographs (as in figure 36).

Fig. 41 Maximum Sr Penetration Depth vs. Joining Temperature and Time for SAS-5 Wetted Si_3N_4 [data presented at 0 min (0 penetration) are inferred and do not reflect actual measurements]
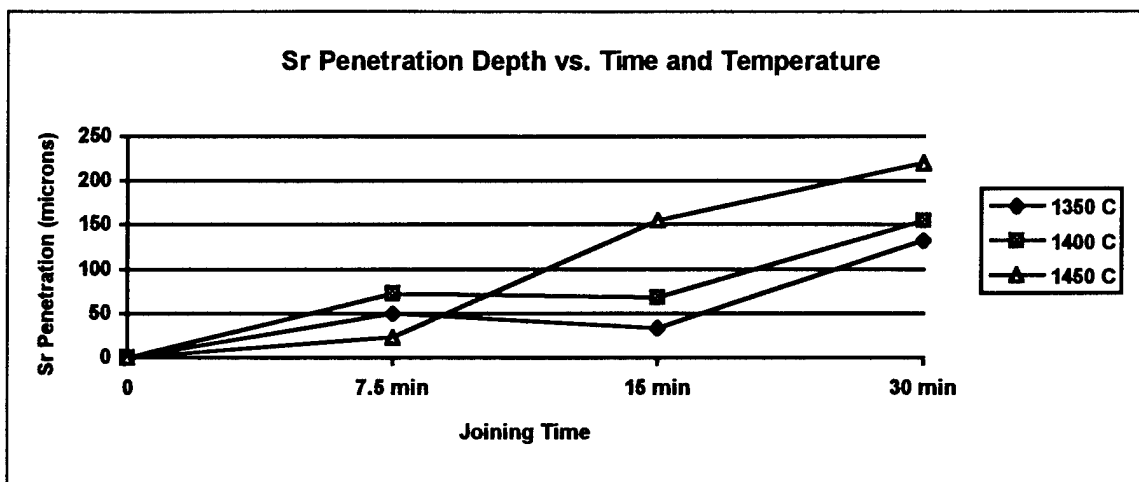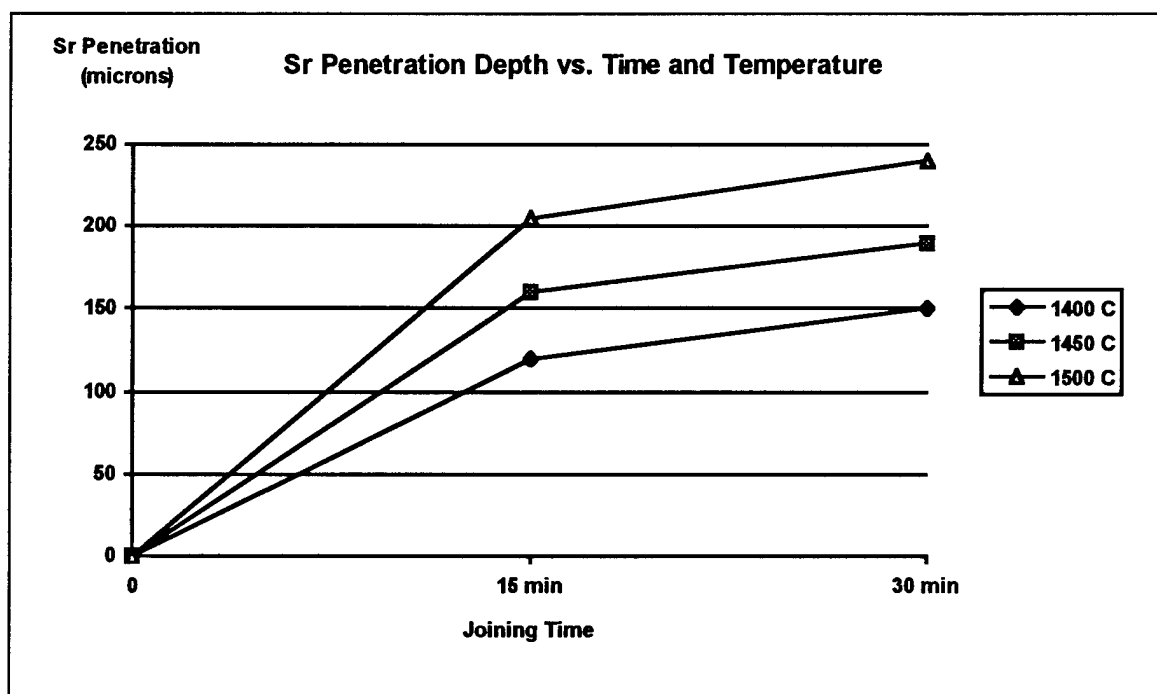

Fig. 42 Maximum Sr Penetration Depth vs. Joining Temperature and Time for SAS-10 Wetted Si_3N_4 [data presented at 0 min (0 penetration) are inferred and do not reflect actual measurements]

This diffusion of Sr ions into the Si_3N_4 is accompanied by a diffusion of Y ions from the Si_3N_4 grain boundary into the molten glass. This diffusion is characterized by a depletion zone at the glass/ Si_3N_4 interface which, in some cases, drops the Y_2O_3 concentration close to 0 wt %. The width of this depletion zone, defined as the distance from the initial drop in concentration on the Si_3N_4 side to the subsequent rise in concentration on the glass side of the interface, is also dependent on wetting temperature, as shown in figures 43 and 44. Since the initial glass compositions were free of Y_2O_3, electron microprobe results reveal Y diffusion throughout the glass region, tapering off to concentrations of less than 2 wt% at the outer limit of the glass. This yields maximum penetration depths for Y diffusion of greater than 250 μm (as in figure 29). This diffusion pattern is also evident in Y elemental diffusion maps (as in figure 35).
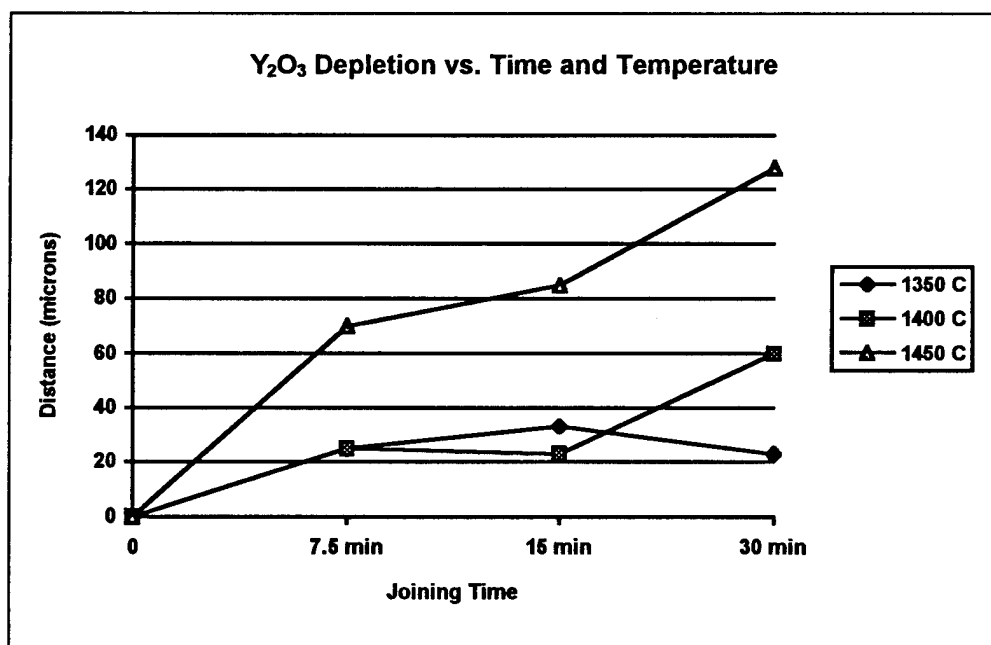

Fig. 43 Y_2O_3 Depletion in SAS-5 Wetting of Si_3N_4 vs. Time and Temperature [data presented at 0 min (0 distance) are inferred and do not reflect actual measurements]

Fig. 44 Y₂O₃ Depletion in SAS-10 Wetting of Si₃N₄ vs. Time and Temperature [data presented at 0 min (0 distance) are inferred and do not reflect actual measurements]
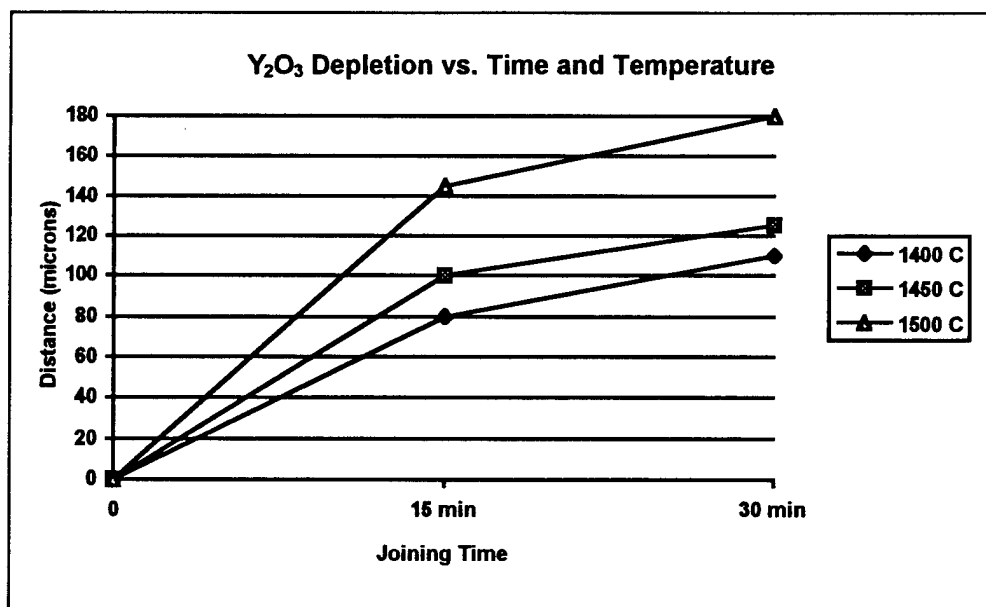
This counter-diffusion of Sr^{2+} and Y^{3+} ions is controlled by conservation of charge in the diffusion zone. This can be seen in magnification of microprobe scans across the interface (figure 45). In this microprobe analysis of SAS-5 wetting Si₃N₄ at 1400 °C for 15 min, the concentration of Y^{3+} ions drops from 3.2 to 1.6 wt % across the 75 to 85 μm range. The Sr^{2+} ion concentration across this range increases from 4 to 6.4 wt%; Al^{3+} concentration remains constant. This correlates to a decrease in Y^{3+} content of 0.018 moles and an increase in Sr^{2+} content of 0.027 moles. These changes are in line with a diffusion of 2 Y^{+3} for every 3 Sr^{+2} ions to maintain ionic neutrality in the region.

Since Al₂O₃ is present in both the glass and grain boundary phase, the driving force for its diffusion is relatively low. The absence of Al₂O₃ diffusion in SAS-10 wetting can possibly be attributed to a saturated Si₃N₄ grain boundary phase. The strong diffusion patterns of Sr^{2+} and Y^{3+} ions, however, driven by concentration gradients and controlled by the conservation of ionic charge, serve as one of the two bonding mechanisms.
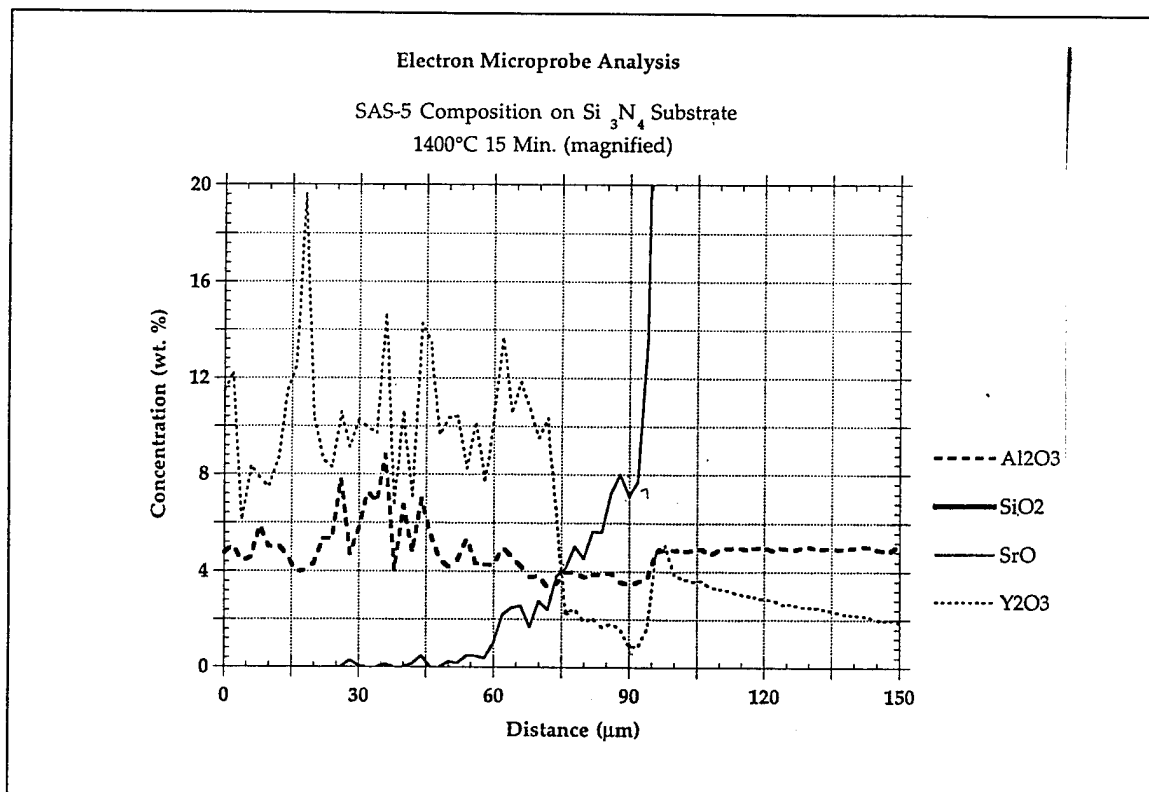
Fig. 45 Magnified electron microprobe analysis of the diffusion zone in SAS-5 wetted Si₃N₄ at 1400 °C for 15 min, showing counter-ion diffusion.

5.4 Chemical Reactions

Mecartney, Sinclair and Loehman (16) reported dissolution of Si_3N_4 at the interface with a molten $MgO-Al_2O_3-SiO_2$ glass and subsequent penetration by the glass into the Si_3N_4. This was then followed by crystallization of Si_2N_2O via:

$$SiO_2(l) + Si_3N_4 \rightarrow 2Si_2N_2O$$

This mechanism resulted in a joint characterized by amorphous and interlocking Si_2N_2O crystalline regions. Although XRD analysis of the 50 μm reaction layer after wetting of the Si_3N_4 by SAS-5 and SAS-10 samples showed no evidence of Si_2N_2O crystals, it did reveal an amorphous region together with β- Si_3N_4 (as in figures 31 and 32).

Furthermore, a BSE image of SAS-10 wetting at 1500 °C, compared to a BSE image of SAS-5 wetting at only 1350 °C, clearly shows signs of Si3N4 surface penetration by the glass (figures 46 and 47). Black particles in the SAS-10 wetting are either precipitated crystals (possibly Si2N2O) or partially dissolved Si3N4 grains.
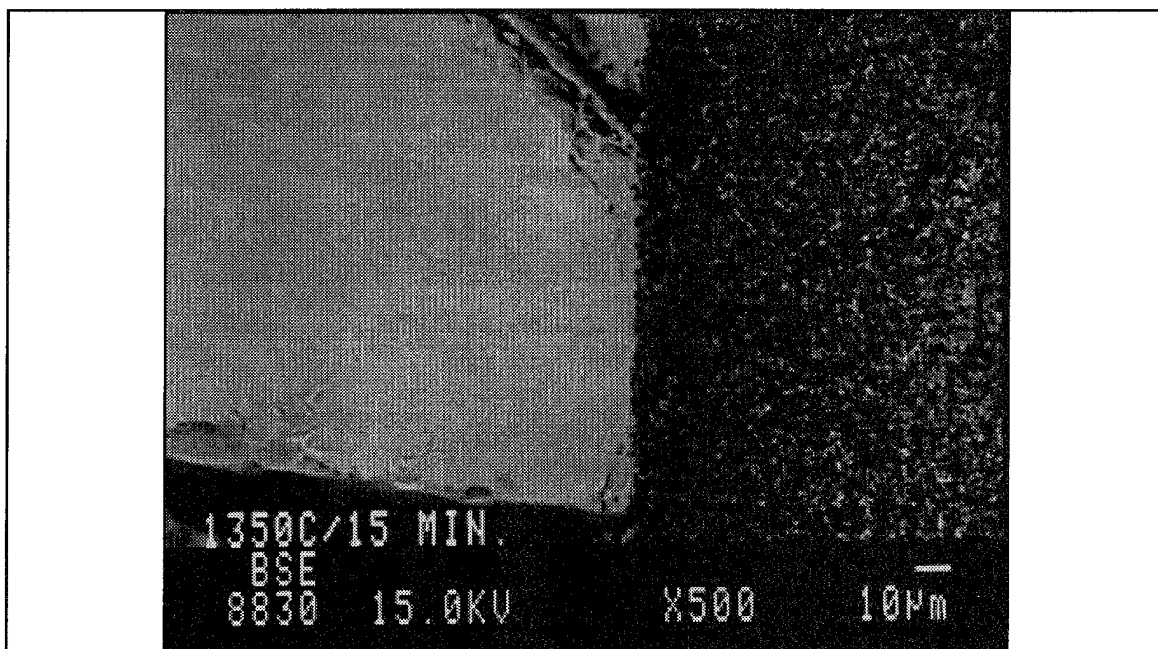

Fig. 46 BSE image of SAS-5 wetting Si3N4 at 1350 °C for 15 min (magnification : 500x) [glass is left of substrate]. Note the relative uniformity of the Si3N4 / glass interface.
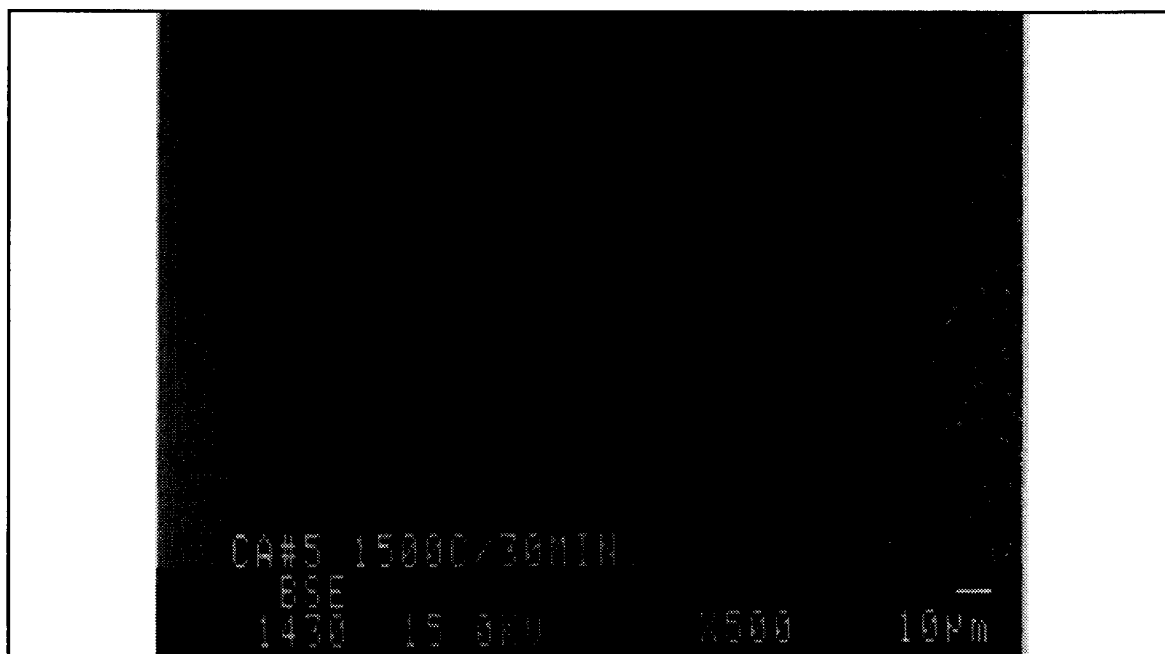
Fig. 47   BSE Image of SAS-10 Composition Wetting Si3N4 at 1500 °C for 30 min (magnification :   500x)   [glass is left of substrate].   Note the black particles that appear to have either precipitated in the glass region or broken off from the Si3N4 substrate.

5.5   Diffusivity Analysis

The diffusion of Sr^{2+} into the Si3N4 grain boundary phase can be analyzed to estimate the diffusion coefficient (D_{Sr}). This estimate is obtained by setting the maximum Sr^{2+} penetration distance equal to $(D_{Sr} \times t)^{1/2}$, where t is the time for diffusion. Electron microprobe results can be used to plot the maximum Sr^{2+} penetration distance (d) vs. $t^{1/2}$ (as done in figures 48 and 49). A straight line in these plots is indicative of diffusion controlled penetration. The slope of these lines yields the value of $(D_{Sr})^{1/2}$ for each joining temperature. For SAS-5 wetting, only the 1450 °C measurements provided good data to obtain a straight line. For SAS-10 wetting, all three joining temperatures (1400 °C, 1450 °C, and 1500 °C) provided good data.
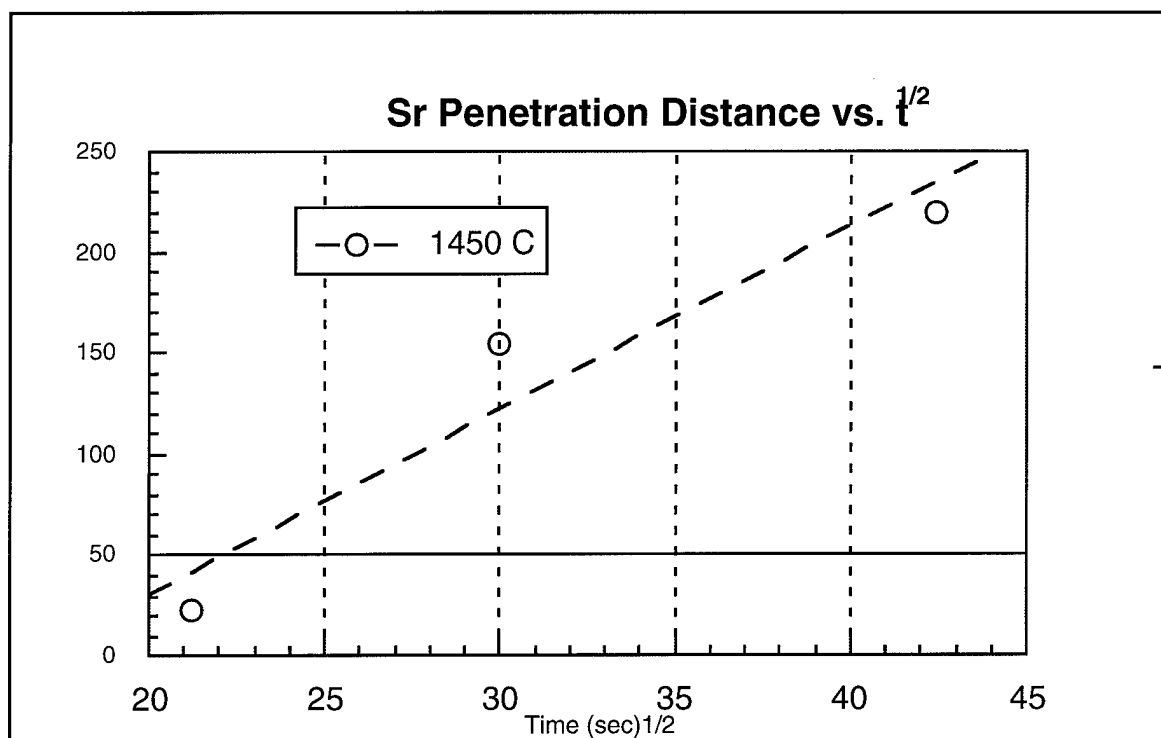
Fig. 48 Maximum Sr^{2+} Penetration vs. $t^{1/2}$ for SAS-5 Wetting at 1450 °C
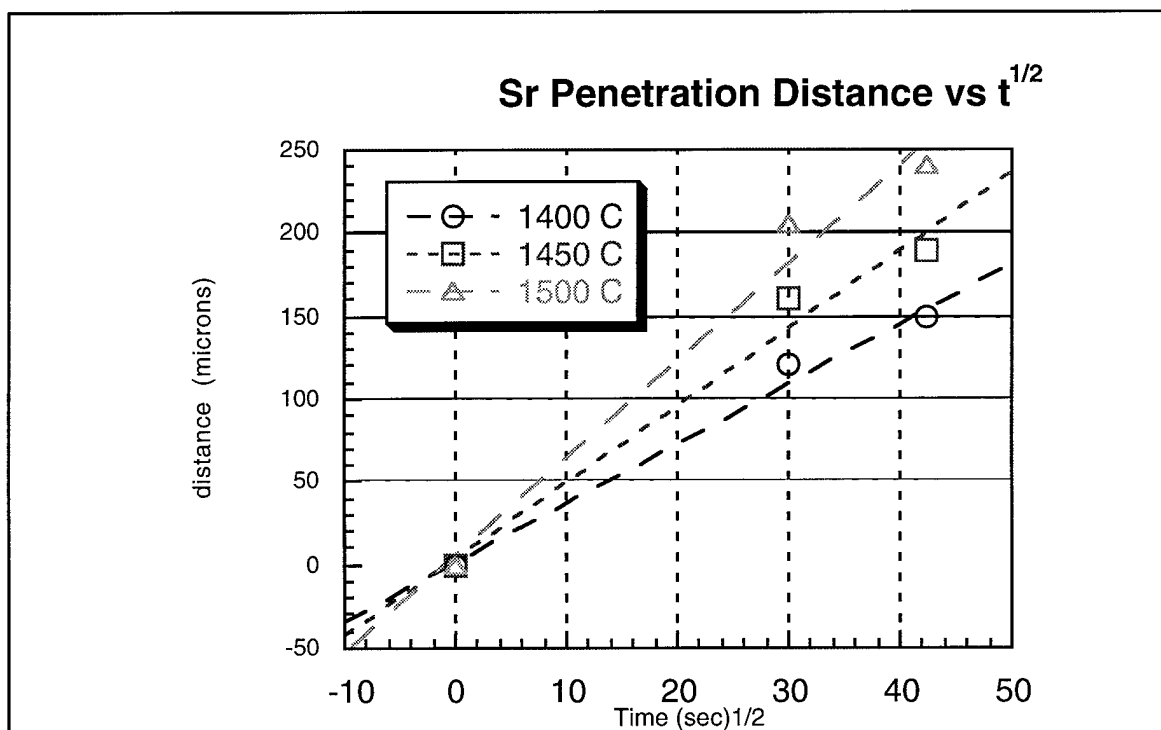
Fig. 49 Maximum Sr^{2+} Penetration vs. $t^{1/2}$ for SAS-10 Wetting [data points at $t^{1/2} = 0$ (0 distance) are inferred and do not reflect actual measurements]

The slopes of these lines yield the following results for diffusion coefficients. In SAS-5 penetration of the Si_3N_4 at 1450 °C, D_{Sr} is measured as 8.1×10^{-7} cm^2/sec. For SAS-10 penetration of the Si_3N_4, D_{Sr} values measured for the three joining temperatures were:

1400 °C - $D_{Sr} = 1.27 \times 10^{-7}$ cm^2/sec

1450 °C - $D_{Sr} = 2.25 \times 10^{-7}$ cm^2/sec

1500 °C - $D_{Sr} = 3.46 \times 10^{-7}$ cm^2/sec

These results compare favorably with the value of $D_{Ca} = 3.4 \times 10^{-6}$ cm^2/sec reported for Ca self-diffusion at 1540 °C in a 38.5 CaO • 21 Al_2O_3 • 40.5 SiO2 melt (*32*).

5.6 Joint Strength

Room temperature joint strengths achieved using SAS-10 and SAS-5 glass interlayers are encouraging for several reasons. The maximum room temperature strength of 470 MPa, attained using SAS-5 glass, is approximately 55% of the room temperature flexure strength of the parent hot-pressed Si_3N_4 plates. Observation of the fractured test bars indicates that full coverage of the Si_3N_4 by the glass was a major factor in the differing strengths, and especially the low strengths. The joining was carried out in the middle of the joining spectrum for the SAS-10 glass; use of a higher joining temperature will likely provide for more fluidity in the glass and subsequently more coverage of the Si_3N_4. Joining was carried out at the upper end of the joining temperature spectrum in the SAS-5 joining. Although coverage appeared more adequate, it was inconsistent along the length of the joint. More control and more even application of the glass powder prior to joining should result in better coverage.

Also, careful attention to the thickness of the joint region should improve the joint strength. Johnson and Rowcliffe (17) reported that joint strength was heavily dependent on this joint thickness, with the optimum thickness being between 20 and 40 μm. The fact that the maximum strength was achieved at the end of the joined plates (for SAS-10 joining) and in the middle of the joined plates (for SAS-5 joining) is indicative of poor coverage, possibly resulting from uneven joint thickness.

5.7 Overview

The glasses studied exhibit good wetting characteristics and present useful mechanisms for joining Si_3N_4 plates. The temperature regimes for the different behavioral patterns for the two compositions are presented in figures 50 and 51. These figures indicate the temperature ranges for good wetting behavior as well as any crystallization. They serve as the foundation for any future evaluation and testing using this glass to join Si_3N_4.

Temperature Behavior for Joining Using SAS-5 Glass

optimum joining range

Decomposition of SiO₂

counter diffusion of cations

Crystallization of glass

1000   1100   1200   1300   1400   1500   1600   C
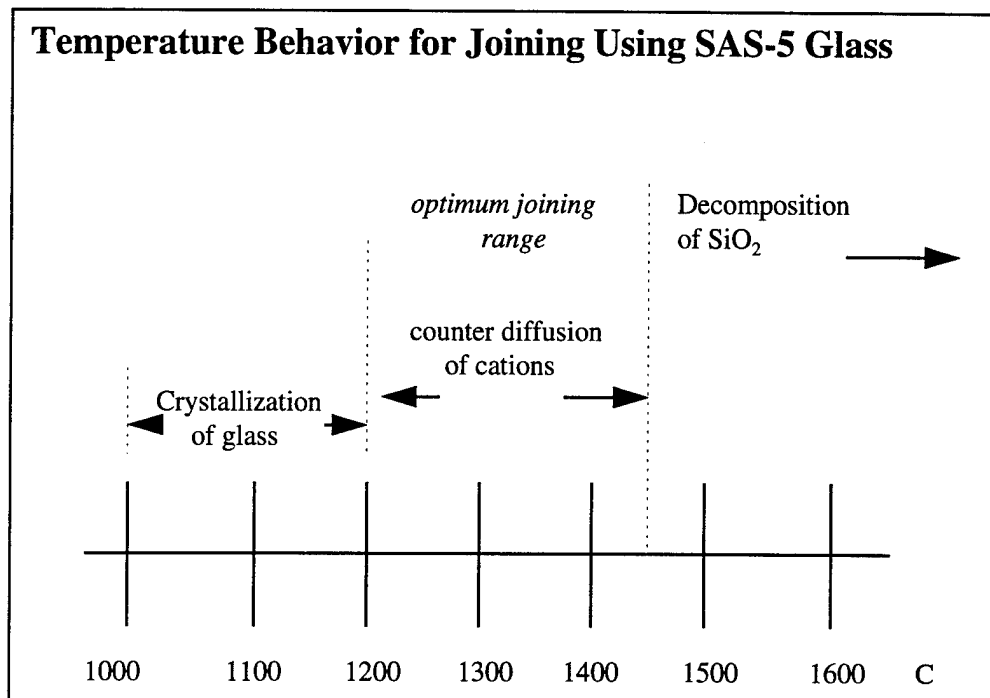
Fig. 50. SAS-5 High Temperature Behavior and Optimum Joining Range

Temperature Behavior for Joining Using SAS-10 Glass

optimum joining range

Decomposition of SiO₂

counter diffusion of cations

No Crystallization of glass

1000   1100   1200   1300   1400   1500   1600   C

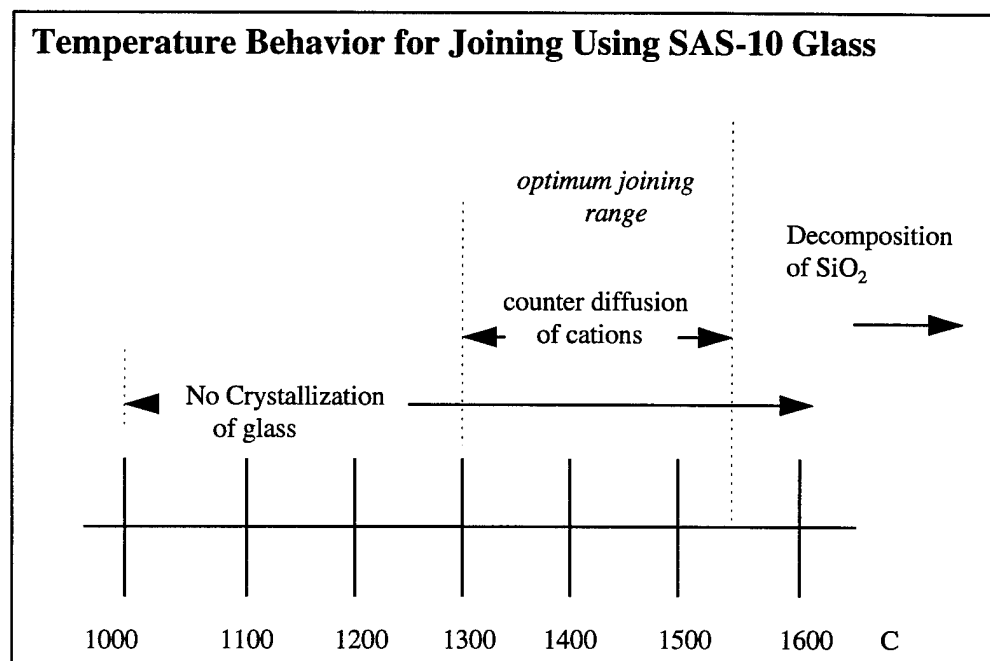**Fig. 51 SAS-10 High Temperature Behavior and Optimum Joining Range**

6 CONCLUSIONS

The SiO_2-SrO-Al_2O_3 system provides a very promising means of joining Si_3N_4 with Al_2O_3 and Y_2O_3 densification aides. In the temperature range of 1300 to 1500 °C, the two glasses studied in this research demonstrated excellent wetting behavior and provided fluidity to cover the Si_3N_4 substrates. Above 1500 °C, the glasses demonstrated increased volatility as SiO_2 decomposition reactions began. The primary mechanisms for bonding were the counter-diffusion of ions between the glass compositions and the intergranular region in the Si_3N_4 as well as the dissolution of Si_3N_4 grains at the interface.

The 470 MPa maximum strength achieved using this glass system (with the SAS-5 composition) is encouraging in terms of the system's potential. Use of higher joining temperatures and increased process control should aide in increasing joint strength. Furthermore, the crystallization of celsian in the SAS-5 composition holds promise for potential high temperature strength. In future work, controlling and optimizing the thickness of the joint region, as well as optimizing the joining temperature to ensure adequate fluidity of the molten glass, should provide for increased room temperature strengths. Once these strengths are attained, focusing on the crystallization of celsian in the joint region could hold the clue to achieving excellent high temperature strengths.

The objective of this research was to determine the bonding mechanisms and thermal stability of the SiO_2-SrO-Al_2O_3 system. This analysis is the preliminary step in evaluating the use of this system in attaining sufficient high temperature joint strengths in Si_3N_4. The room temperature strengths achieved using these glasses are important in terms of demonstrating that the system can provide good joint strengths. However, the real utility of this glass system will be seen in its ability to provide crystalline celsian in the joint and achieve an excellent CTE match across the interface.

REFERENCES

1) J. T. Neil, "The Big Three in Structural Ceramics", *Materials Engineering*, **99**, 3 (1984).

2) D. J. Godfrey, "The Use of Ceramics in Diesel Engines", in Nitrogen Ceramics, *Proceedings of the NATO Advanced Study Institute on Nitrogen Ceramics 1976*, edited by F. L. Riley, Noordhoff International Publishing.

3) G. S. Brady, H. R. Clauser, Materials Handbook, 13th edition, McGraw-Hill Inc., New York, 1991.

4) R. N. Katz, "Applications of Nitrogen Ceramics--Gas Turbines: U.S. National Programs" in Nitrogen Ceramics, *Proceedings of the NATO Advanced Study Institute on Nitrogen Ceramics 1976*, edited by F. L. Riley, Noordhoff International Publishing.

5) J. A. Salem, J. M. Manderscheid, M.R. Freedman, J. P. Gyekenyesi, "Reliability Analysis of a Structural Ceramic Combustion Chamber", NASA Technical Memorandum 103264 (1991).

6) H. G. Gibson, "An Evaluation of Bearings Operating in a Cryogenic Environment with Silicon Nitride Rolling Elements", NASA Technical Memorandum 103524 (1991).

7) E. Gugel, "A Consideration of Some Silicon Nitride Applications" in Nitrogen Ceramics, *Proceedings of the NATO Advanced Study Institute on Nitrogen Ceramics 1976*, edited by F. L. Riley, Noordhoff International Publishing.

8) K. Suganuma, T. Okamoto, M. Koizumi, M. Shimada, "Joining of Silicon Nitride to Silicon Nitride and to Invar Alloy Using an Aluminum Interlayer", *J. Materials Sci.* **22** (1987).

9) M.E. Milberg, H. D. Blair, W. T. Donlon, S. S. Shinozaki, "The Nature of SiAlON Joints Between Silicon Nitride Based Bodies", *J. Materials Sci.* **22** (1987).

10) T. Kaba, M. Shimada, M. Koizumi, "Diffusional Reaction-Bonding of Si_3N_4 Ceramics Under High Pressure", *Comm. of Amer. Ceramics Soc.* **66**, 8 (1983).

11) M. Nakamura, K. Kubo, S. Kanzaki, H. Tabata, "Joining of Silicon Nitride Ceramics by Hot Pressing", *J. Materials Sci.* **22** (1987).

12) M. Nakumra, S. D. Peteves, "Joining of Silicon Nitride Ceramics Under Nitrogen Gas Pressure", *J. Materials Sci. Letters* **8**, 10 (1989).

13) G. J. Sundberg, M. K. Ferber, "Joining of Silicon Nitride for Heat Engine Applications", *Ceramic Engr. Sci. Proceedings* **10**, 7 (1989).

14) O. Akselsen, "Review: Diffusion Bonding of Ceramics", *J. Materials Sci.* **27** (1992).

15) P. F. Becher, S. A. Halen, "Solid-State Bonding of Si_3N_4", *Bulletin of Amer. Ceramics Soc.* **58**, 6 (1979).

16) M. L. Mecartney, R. Sinclair, R. E. Loehman, "Silicon Nitride Joining", *J. Amer. Ceramic Soc* **68**, 9 (1985).

17) S. M. Johnson, D. J. Rowcliffe, "Mechanical Properties of Joined Silicon Nitride", *J. Amer. Ceramic Soc* **68**, 9 (1985).

18) N. Iwamoto, N. Umesaki, Y. Haibara, " Silicon Nitride Joining with Glass Solder in the $CaO-SiO_2-TiO_2$ System" in Fundamentals of Diffusion Bonding, edited by Y. Ishida, Institute of Industrial Science, University of Tokyo (1987).

19) K. Okida, H. Takai, T. Nishi, H. Yanagida, "Electrical Joining of Silicon Nitride Ceramics", *J. Amer. Ceramic Soc* **76**, 6 (1993).

20) M. H. O'Brien, "Joining of Silicon Nitrides Using Oxynitride Glasses", Idaho National Engineering Laboratory Contractor Memorandum 10713 (1993).

21) H. Takeuchi, Y. Takano, A. Yamakawa, M. Miyake, "Joining of Silicon Nitride Ceramics", *Tokyo Fine Ceramics* March (1993).

22) P. A. Walls, M. Ueki, "Mechanical Properties of β-SiAlON Ceramics Joined Using Composite β-SiAlON-Glass Adhesives", *J. Amer. Ceramic Soc* **78**, 4 (1995).

23) A. F. McLean, R. R. Baker, "Brittle Materials Design, High Temperature Gas Trubine", Army Materials and Mechanics Research Center, U.S. Government Report No. AMMRC-TR-78-14 (1978).

24) Phase Diagrams for Ceramicists, American Ceramic Society (1975).

25) N.P. Bansal, M. J. Hyatt, "Crystallization and Properties of Sr-Ba Aluminosilicate Glass-Ceramic Matrices", *Ceramic Engr. Sci. Proceedings* **12**, 7-8 (1991).

26) C.H. Drummond III, W.E. Lee, N.P. Bansal, M.J. Hyatt, "Crystallization of a Barium-Aluminosilicate Glass", *Ceramic Engr. Sci. Proceedings* **10**, 9-10 (1989).

27) N. P. Bansal, C.H. Drummond III, "Kinetics of Hexacelsian-to-Celsian Phase Transformation in $SrAl_2Si_2O_8$", *J. Amer. Ceramic Soc* **76**, 5 (1993).

28) L. Barbieri, A. Bomartini Corradi, C. Leonelli, T. Manfredini, M. Romagnoli, C. Siligardi, "The Microstructure and Mechanical Properties of Sintered Celsian and Strontium-Celsian Glass-Ceramics", *Materials Res. Bulletin* **30**, 1 (1995).

29) J. A. Pask, A. P. Tomsia, "Wetting, Surface Energies, Adhesion, and Interface Reaction Thermodynamics" in Engineered Materials Handbook, Vol. 4, Ceramics and Glasses, ASM International (1991).

30) W. F. Chambers, "BA85: A Bence-Albee Oxide Analysis Routine with Mineral Code Capabilities", SAND90-1702, Sandia National Laboratories, Jan 1991.

31) MIL-STD 1942A "Flexural Strength of High Performance Ceramics at Ambient Temperatures", U.S. Army Materials Technology Lab, Watertown, MA (1990).

32) H. Towers, J. Chipman, "Diffusion of Calcium and Silicon in a Lime-Alumina-Silica Slag", *Trans. AIME*, **209**, 769-773 (1957).